Energy-conserving spectral element schemes based on Lagrangian dynamics

Investigating discrete energy conservation

Wessel Niek Weijers

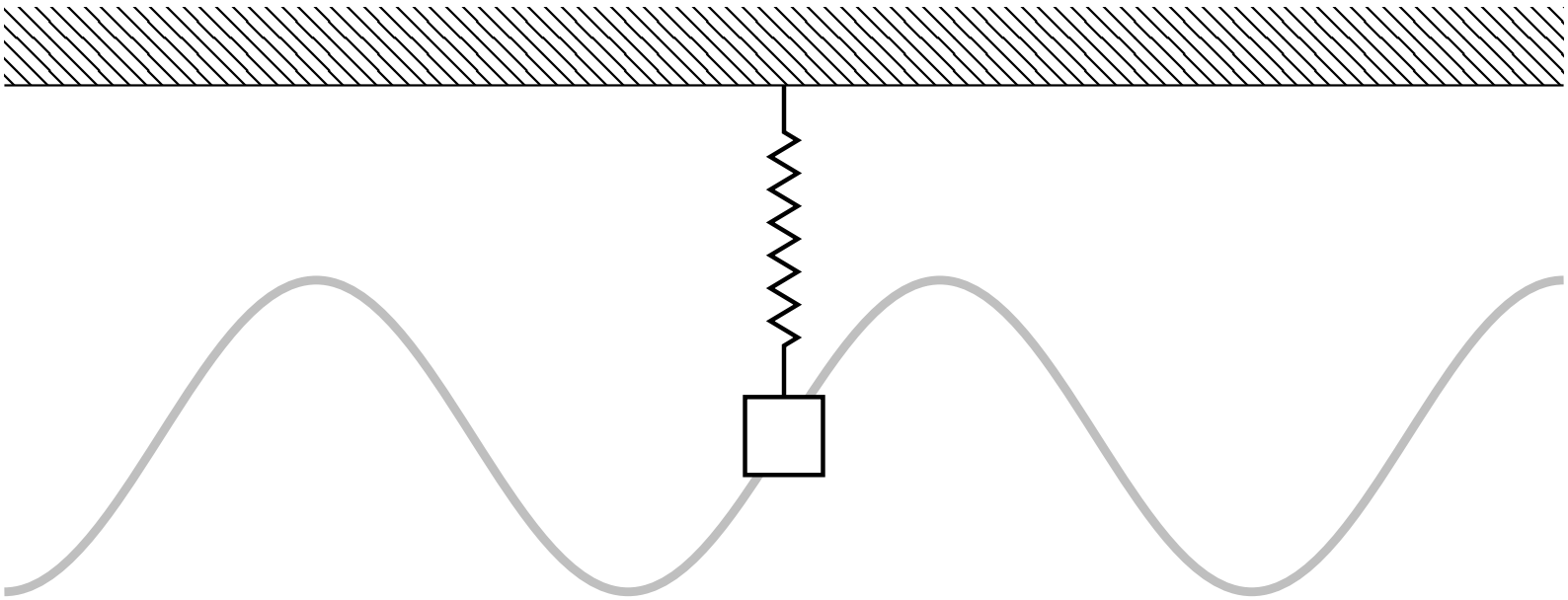

TU Delft

Energy-conserving spectral element schemes based on Lagrangian dynamics

Investigating discrete energy conservation

by

Wessel Niek Weijers

to obtain the degree of Master of Science
at the Delft University of Technology,
to be defended publicly on Friday January 31, 2020 at 10:00 AM.

Student number:	4353730	
Project duration:	February 20, 2019 – January 31, 2020	
Thesis committee:	Dr. ir. M.I. Gerritsma,	TU Delft, supervisor
	Dr. ir. A.H. van Zuijlen,	TU Delft
	Dr. H.M. Schuttelaars,	TU Delft
	Ir. V. Jain	TU Delft

An electronic version of this thesis is available at `http://repository.tudelft.nl/`.

TU Delft

Summary

Physical systems in the continuous domain are often solved using computer-aided software because of their complexity. Preserving the physical quantities from the continuous domain in the discrete domain is therefore of utmost importance. There is however a broad range of techniques that can accomplish the translation between the continuous and discrete domain, e.g. finite difference, volume and element techniques, fourth order Runge-Kutta or Störmer-Verlet to name a few. Accompanied with the aforementioned come strengths and weaknesses but have the common thread to try maintaining the physical behaviour of the continuous system closely. The mimetic spectral element technique is used to develop an energy-conserving spectral element scheme through a Lagrangian formulation. This new formulation of the mimetic spectral element technique allows for solving time-dependent problems and the simple harmonic oscillator serves as the sample problem in this thesis.

The solution has been derived from Lagrangian mechanics in a variety of ways. Discrete Lagrangian formulations have been investigated at first and their respective equations of motions have been tested against the exact solution of the simple harmonic oscillator. This method achieved marching in time and no damping of the solution, yet energy was only bounded and not exactly conserved. The mimetic spectral element formulation of the Lagrangian formulation showed difficulties when using variational analysis, i.e. boundary treatment in the future. Arbitrary domain mapping was among the possible solutions, but this formulation was found to be unreliable and unsuccessful. It was found that a more robust formulation, i.e. the spectral marching method, was most suitable.

Throughout this thesis the focus was put on the conservation of energy using a Lagrangian formulation. Except the spectral scheme using arbitrary domain mapping, all schemes kept the energy of the system bounded, but no energy was conserved up to machine precision. Using arbitrary domain mapping, the energy seemed to grow over time.

Acknowledgements

I never realised the importance of discretisation techniques until I started my thesis. I was aware that bridging the gap between real life and simulation could be done in a variety of ways and that with each method came both desired and undesired consequences. During my last course in aerospace engineering at Delft University of Technology, I got acquainted with a new discretisation technique, i.e. the mimetic spectral element method. Recognising the potential of this new theory, I asked the lecturer - my supervisor - about graduation topics. When he replied with the question to solving time-dependent problems using the mimetic spectral element technique, I got enthusiastic and accepted the challenge.

And what a challenge it was. Various methods were tried but, like I mentioned earlier, those undesired consequences often brought me back to the drawing board. Despite the latter, I am grateful to what this thesis has brought me and proud of the document that lies in front of you.

Without the support of my supervisor, dr.ir. M.I. Gerritsma, this thesis would not have been possible. Marc, I appreciated your help at any time, your support and your dedication to the problem. Furthermore, I would like to thank Varun Jain and Yi Zhang, PhD candidates of the aerodynamics group at Delft University of Technology for their help and support. Like Marc, they always took time to help me with whatever I was having problems with.

Lastly, I would like to thank my friends and family but in particular my girlfriend. Daniëlle, without your support and encouragement at home, I would never have finished my thesis. Also, thank you for the good discussions we had on the topic whenever I got stuck.

To the one that takes my thesis as a baseline and continuous with time-dependent problems in combination with the mimetic spectral element technique, all the best of luck. All that remains for me to say is that I look back on a good learning process and that I am ready to take on new challenges that lie ahead.

Wessel Niek Weijers
Delft, January 21, 2020

Nomenclature

I	time instant	
L	line	
P	point	
S	surface	
T	time interval	
V	volume	
α	infinitesimal increment factor	
β	infinitesimal increment factor	
δ	variational analysis operator	
$\mathcal{R}$	reduction operator	
π	projection operator	

Constants

A	amplitude	m
b	end time	s
c	constant	
d	constant	
k	spring stiffness	$\mathrm{N\,m^{-1}}$
m	mass	kg
n_e	number of elements	
p	polynomial degree	
r	constant	

Continuous quantities

a	start time	s

b	end time	s
$E(t)$	total energy	J
$e_i(t)$	edge basis function	
$H(p, x)$	Hamiltonian	J
$h_i(t)$	nodal basis function	
$L(x, \dot{x})$	Lagrangian	J
$l_i(\tau)$	Lagrange polynomial	
$L_p(t)$	Legendre polynomial	
$p(t)$	momentum	$\mathrm{kg\,m\,s^{-1}}$
$S(p, x)$	action	$\mathrm{J\,s}$
$T(\dot{x})$	kinetic energy	J
t	time variable	s
$v(t)$	velocity	$\mathrm{m\,s^{-1}}$
$V(x)$	potential energy	J
$x(t)$	position variable relative to datum	m

Discretised quantities

Δt	time interval	s
$\mathbb{E}$	incidence matrix	
$\mathbb{K}$	spring stiffness matrix	$\mathrm{N\,m^{-1}}$
$\mathbb{M}$	mass matrix	kg
$\mathcal{E}$	edge basis vector	
$\mathcal{H}$	nodal basis vector	
E_i	total energy	J
p_i	(conjugate) momentum	$\mathrm{kg\,m\,s^{-1}}$
t_i	discrete time	s
x_i	position	m

Subscripts and superscripts

$\bar{\square}$	inner orientation
$\ddot{\square}$	double time derivative
$\dot{\square}$	single time derivative

$\square'$ dual equivalent of primal basis function

$\square^h$ reconstructed quantity

$\square_0$ initial value

$\square_i$ index

$\square_j$ index

$\hat{\square}$ known value

$\tilde{\square}$ outer orientation

$\vec{\square}$ vector quantity

List of Figures

List of Tables

Contents

1 Introduction

Everyone remembers him- or herself at the playground swaying back and forth on a swing. Would you not have moved your legs, eventually you would have come to a standstill. By swaying your upper body and legs at the right moment, the swing kept going.

The event above is a clear, everyday example of a forced oscillator with damping. Lets pretend that you do not move your legs and upper body and you stop swinging after some time due to friction in the hinge above your head. The system's energy is dissipated from the swing and transformed into frictional energy, i.e. heat. Without the presence of friction, you would have swung eternally.

1.1 Reason behind the choice of topic

Neglecting friction constitutes the simple harmonic motion that conserves energy and continues forever. This real world example can be represented mathematically by means of an ordinary differential equation. Its exact solution is widely known and can be analytically derived as shown in Appendix A. The total energy of the system can also be calculated and can be shown to be constant. A similar result is desired when treating this system at discrete level. However, even for the simple problem mentioned above, discretising the continuous system is accompanied with a loss of physics, i.e. energy may not be conserved. This means that bridging between the continuous problem and the discrete problem is accompanied with a loss of information.

The example described above is a graspable example that everyone understands. There are however many more applications that benefit from conserving energy at a discrete level. Think for instance about fluid-structure interactions such as wing tip flutter. This example requires the coupling between fluid and structure, with energy transfer from one to another. Calculating the energy level too inaccurate means the other system lacks behaviour and so it continuous.

Another field of research that plays an important role in society nowadays is aeroaccoustics. The field of aeroaccoustics also benefits from good energy behaviour and energy conservation. Analyses involving sound go together with energy levels and therefore can only deliver meaningful analyses when energy calculations are done properly. Furthermore, the computations of many of these problems are done using computational fluid dynamics software, dealing with chaotic, oscillatory or laminar flow.

As a result, many discretisation techniques have been developed to mimic the continuous system as accurately as possible, yet still taking the loss of information for granted. This thesis however, focuses on the use of a relatively new discretisation technique, i.e. the mimetic spectral element technique. Using this technique it is attempted to keep an important part of real physics intact at discrete level, i.e. to conserve energy. The reader may however still not be convinced about the necessity to conduct research on yet a new discretisation technique as there exist many different techniques already. The problem with many of the discretisation techniques however, is the diverging behaviour of the solution over a long period, i.e. artificial damping. This might result in problems, considering the wing tip flutter example mentioned

above.

1.2 Research objective and research questions

The mimetic discretisation technique that will be evaluated has a promising history already. The mimetic spectral element method has been applied to steady differential systems in one- and multi-dimensional spaces. These steady systems however, had the benefit of being independent of time. The theoretical development of the mimetic spectral element problem to time-dependent problems is the next step forward but faces some challenges. Without discussing the details of these challenges, a small explanation is given. Unlike discretising space and its boundary conditions, time is only bounded at one side. One would otherwise restrict the future to a solution and solve only for what happens in-between the two time instants. This will be explained more thoroughly in Section 2.3. To be precise, this thesis aims

Research Objective

> to further develop the mimetic spectral element method in its fourth dimension time by critically reflecting on the core concepts of differential topology, algebraic topology and mimetic operators of the mimetic spectral element method and Lagrangian and Hamiltonian mechanics.

Hand-in-hand with the research objective come research questions. The research questions are stated below and will again be reflected on in Chapter 5. Chapter 5 will also answer the research objective.

Research Questions

1) How does time-dependence fit in the mimetic spectral element method?

2) Why have not yet other engineers tried (or succeeded) to solve time-dependent problems using the mimetic spectral element method?

3) Is it possible to discretise time in a similar way as space is discritsed according to the mimetic spectral element method?

In this report, it is attempted to answer the above stated research objective and questions. Furthermore, this report contributes to science by means of different derivations (e.g. Equation (4.7)) and insights to use the mimetic spectral element method for time-dependent problems (e.g. Sections 4.3 and 4.5).

1.3 Thesis outline

A concise literature review is provided in Chapter 2. It is found that few others dealt with the same concept and tackled the problem using different perspectives. The mathematical building blocks are described Chapter 3. Subsequently, the theories are then applied in Chapter 4 to a fundamental problem in the field of mechanics, i.e. the simple harmonic oscillator. The problem is approached with a variational integrator technique in Section 4.2 and known linear and arbitrary linear $t - \tau$ mapping in Sections 4.3 and 4.4 respectively. The best results from Sections 4.3 and 4.4 are taken together and a new spectral marching method is described in Section 4.5. A conclusion is provided in Chapter 5 after which future work recommendations are proposed in the same chapter.

2 Literature review

In spite of the mimetic spectral element method being relatively new, its fundamental concept can be traced back to 1971 [1]. The relation between geometric objects and physical quantities was first researched in [1]. This relation meant for instance the connection between position in space and nodal points but also the connection between velocity and line segments, as

$$\int_{t^i}^{t^{i+1}} [\vec{v}(t)]\ dt = \vec{x}(t^{i+1}) - \vec{x}(t^i) \tag{2.1}$$

indicates that velocity is nothing else but the difference between two spatial points divided by the time difference [2]. Although the example above might be obvious, in [1] it is concluded that to every physical quantity a geometric object is related. With this concept in mind and a proper choice of nodes and basis functions, the spectral method has evolved to be a powerful discretisation technique. The subsequent paragraphs of this chapter elaborate more on the historical background of the mimetic spectral element technique and the discretisation of time. In Section 2.1 one finds the necessary historical events in chronological order that define the mimetic spectral element method, followed by an enumeration of performed studies in Section 2.2. The history of discretising time is treated in Section 2.3 and other discretisation techniques are elaborated upon in Section 2.4.

2.1 History in chronological order

As was previously mentioned, the concepts by Tonti in [1] created the first building blocks of the mimetic spectral element method. Just as with space, physical quantities that are timelike are also related to objects. Once an orientation is assumed, known as inner- or outer orientation, 32 different relations between space and time are found. Tables 2.1 to 2.4 indicate all possibilities between space and time elements. The spatial possibilities are listed column-wise, whereas the timelike possibilities are listed row-wise. P, L, S and V refer to a point, a line, a surface and a volume in space and I and T represent the time instant and time interval [3]. The inner orientation is represented by $\bar{\square}$ and the outer orientation is indicated by means of $\tilde{\square}$. They indicate whether a quantity moves for instance along a line ($\bar{L}$) or a quantity moving through a surface ($\tilde{S}$). Other inner- and outer orientations are shown in Figure 2.1.

In 1976, [4] was published by Dodziuk in which the importance of "inner products of cochain spaces" was stressed. Later, the potential of the new method was applied to the theory on electromagnetic field problems in [5] and a dual mixed method was established. Bossavit et al. later published a technique that separated metric-dependent and metric-independent operations [6]. The separation of the aforementioned enabled it to narrow the discretisation error to only metric-dependent operations as the metric-independent operations are exact. Lastly, in [7] it was mentioned once more that physical quantities and geometric objects needed to be related to each other by "a common structure".

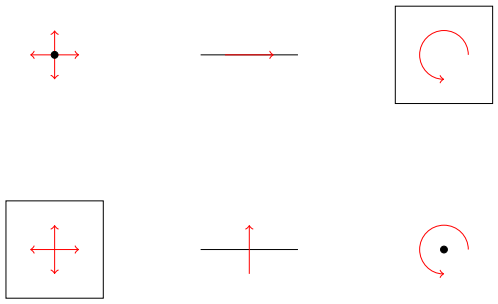

Figure 2.1: Representations of $\bar{P}$, $\bar{L}$ and $\bar{S}$ on the top row indicating inner oriented spatial objects. Representations of outer oriented spatial objects $\tilde{S}$, $\tilde{L}$ and $\tilde{P}$ shown at the bottom row.

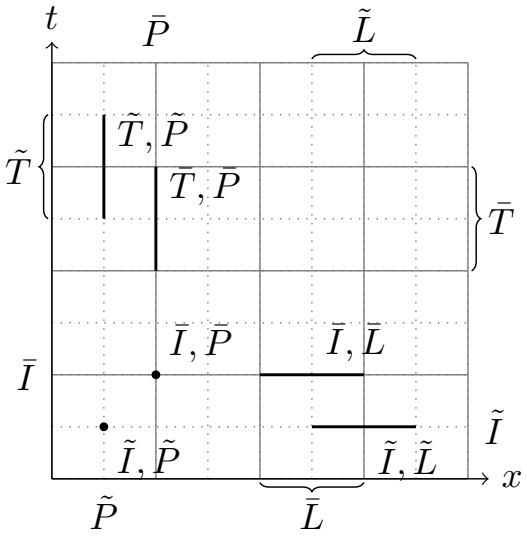

Figure 2.2: Illustrations of various space-time elements.

Table 2.1: Eight oriented space-time elements with inner oriented space and time elements [1, p. 3].

	$\bar{I}$	$\bar{T}$
$\bar{P}$	$[\bar{I}, \bar{P}]$	$[\bar{T}, \bar{P}]$
$\bar{L}$	$[\bar{I}, \bar{L}]$	$[\bar{T}, \bar{L}]$
$\bar{S}$	$[\bar{I}, \bar{S}]$	$[\bar{T}, \bar{S}]$
$\bar{V}$	$[\bar{I}, \bar{V}]$	$[\bar{T}, \bar{V}]$

Table 2.2: Eight oriented space-time elements with outer oriented space and time elements [1, p. 3].

	$\tilde{I}$	$\tilde{T}$
$\tilde{P}$	$[\tilde{I}, \tilde{P}]$	$[\tilde{T}, \tilde{P}]$
$\tilde{L}$	$[\tilde{I}, \tilde{L}]$	$[\tilde{T}, \tilde{L}]$
$\tilde{S}$	$[\tilde{I}, \tilde{S}]$	$[\tilde{T}, \tilde{S}]$
$\tilde{V}$	$[\tilde{I}, \tilde{V}]$	$[\tilde{T}, \tilde{V}]$

Table 2.3: Eight oriented space-time elements with inner oriented space and outer oriented time elements [1, p. 3].

	$\tilde{I}$	$\tilde{T}$
$\bar{P}$	$[\tilde{I}, \bar{P}]$	$[\tilde{T}, \bar{P}]$
$\bar{L}$	$[\tilde{I}, \bar{L}]$	$[\tilde{T}, \bar{L}]$
$\bar{S}$	$[\tilde{I}, \bar{S}]$	$[\tilde{T}, \bar{S}]$
$\bar{V}$	$[\tilde{I}, \bar{V}]$	$[\tilde{T}, \bar{V}]$

Table 2.4: Eight oriented space-time elements with outer oriented space and inner oriented time elements [1, p. 3].

	$\bar{I}$	$\bar{T}$
$\tilde{P}$	$[\bar{I}, \tilde{P}]$	$[\bar{T}, \tilde{P}]$
$\tilde{L}$	$[\bar{I}, \tilde{L}]$	$[\bar{T}, \tilde{L}]$
$\tilde{S}$	$[\bar{I}, \tilde{S}]$	$[\bar{T}, \tilde{S}]$
$\tilde{V}$	$[\bar{I}, \tilde{V}]$	$[\bar{T}, \tilde{V}]$

2.2 Performed studies

There are plenty of studies performed over the recent years that use the mimetic spectral element method. Problems suchs as the the generalised convection-diffusion problems [8], the Darcy's problem [9, 10], Stokes flow [11, 12], the Grad-Shafranov equation [13, 14], anisotropic diffusion [15], elliptic problems [16,17], Hamiltonian systems [18], linear elasticity [19], potential flows [20] and the Laplace's equation [19] are among them. Furthermore, it has been extended to three-dimensional problems, including periodic incompressible Euler flows [21].

Recent performed studies show a growing interest in time-dependency being incorporated in the mimetic spectral element method. Where stationary problems were focused on in the past, time-dependence is increasingly mentioned in future research sections of papers and reports [19, p. 96]. Space-time models have already been treated in the past, see for example [16]. The one-dimensional convection-diffusion equation was treated in [8, p. 19], but lacked significant detail in the treatment of the time variable. Lastly, the paper of Palha, [18], comes closest to the subject of this thesis - applying the mimetic spectral element method to time-dependent problems. Another field of studies that is currently investigated regarding the mimetic spectral element method is the expansion to three dimensional spaces [21].

2.3 Discretisation of time

Recall (2.1), which is an exact relation between position and velocity. Discretising the continuous equation can be done in various ways. Throughout history, different time-marching methods have been created. Among the latter is the discretisation technique that uses a Taylor series approximation. A first order Taylor approximation around t^i can be written as

$$x(t^{i+1}) \approx x(t^i) + \frac{\dot{x}(t^i)}{1!}(t^{i+1} - t^i), \tag{2.2}$$

which mimics (2.1) when rewritten in the form

$$\dot{x}(t^i)\Delta t \approx x(t^{i+1}) - x(t^i), \tag{2.3}$$

which can be deduced from (2.1) when $\vec{v}(t)$ is constant in the interval $t \in [t^i, t^{i+1}]$. The necessity to conduct research in the field of time-dependent problems in combination with the mimetic spectral element method is best explained when looking at (2.2). Assume an exact solution of the form

$$x(t) = 2\cos(t), \tag{2.4}$$
$$v(t) = \dot{x}(t) = -2\sin(t), \tag{2.5}$$

which means that exact position and velocity are known. In Figure 2.3, one finds the exact solution plotted for $t = 0$ until $t = 0.2$. Equation (2.1) suggests that once position and velocity are known at $t = t^i$, $x(t^{i+1})$ can be calculated.

It is directly noticed that the approximated solution does not capture the exact physics of the problem. It is also immediately seen that energy of the discrete system will not be constant

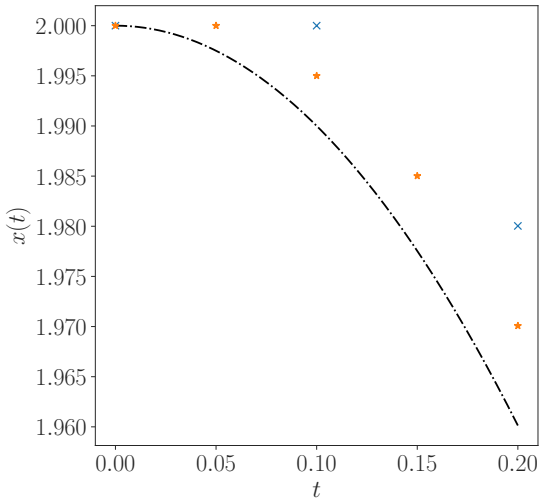

Figure 2.3: Exact and discrete solution of (2.4) with $\Delta t = 0.1$ ($\times$) and $\Delta t = 0.05$ ($*$), $x_0 = x(0)$ and $\dot{x}_0 = \dot{x}(0)$. Exact solution shown as $- \cdot -$. Equation (2.5) is substituted in (2.2).

over time. Recalling (2.4) and (2.5), at a continuous level this system conserves energy through

$$\begin{aligned} E(t) &= \frac{1}{2}x^2(t) + \frac{1}{2}\dot{x}^2(t), \\ &= \frac{1}{2}\left(2\cos(t)\right)^2 + \frac{1}{2}\left(-2\sin(t)\right)^2, \\ &= 2\cos^2(t) + 2\sin^2(t), \\ &= 2, \end{aligned} \tag{2.6}$$

indicating that the energy level is independent of time. In consequence this means that

$$\frac{\mathrm{d}E}{\mathrm{d}t} = 0. \tag{2.7}$$

On the contrary however, this is not the case for the discretised system. The difference between exact and approximated position is an indication that energy will not be conserved. ΔE at discrete follows through

$$\begin{aligned} \Delta E &= E_{i+1} - E_i, \\ &= \frac{1}{2}x_{i+1}^2 + \frac{1}{2}\dot{x}^2(t_{i+1}) - \frac{1}{2}x_i^2 - \frac{1}{2}\dot{x}^2(t_i), \end{aligned} \tag{2.8}$$

which will not be zero for positions x_i. Many researchers have tried capturing the physical behaviour using more sophisticated time discretisation methods, e.g. variational integrators [22] or geometric integrators [23]. Others approach the problem from a different perspective and use Lagrangian mechanics. Noticing explicit time independence, the equations of motion that conserve energy follow [24, 25].

2.4 Other discretisation techniques

Discretisation methods that are widely used nowadays are for example the finite difference method, the finite volume method and the finite element method. The finite difference method approximates the derivative through nodal differences. Together with appropriate boundary

conditions, the finite difference formulation of the original differential equation is found [26]. The finite volume method uses the integral formulation of the differential equation, reducing therefore the order of the problem by one [27]. Lastly, the method known as the finite element method can be seen as one of the predecessors of the mimetic spectral element technique as this technique also requires a functional formulation. Finding its minimum results in the weak formulation of the differential equation and is thereafter solved using basis functions [27].

More sophisticated discretisation techniques suitable for solving ordinary differential equations are for instance the classic Runge-Kutta method or the basic Störmer-Verlet technique. As these techniques are more sophisticated, an explanation follows hereafter. The Runge-Kutta method uses the Euler method to solve differential equations [28]. The most common and most widely known Runge-Kutta method is the fourth order Runge-Kutta method which reads [29]

$$\begin{aligned} \dot{x} &= f(x,t), \\ x(t_0) &= x_0, \end{aligned}$$

and using the discretisation

$$\begin{aligned} x_{i+1} &= x_i + \sum_{i=1}^{4} w_i k_i, \\ k_i &= h_n f\left(x + \alpha_i h_n, t + \sum_{j=1}^{i-1} \beta_{ij} k_j\right), \\ w_1 = w_4 &= \frac{1}{6} \quad \text{and} \quad w_2 = w_3 = \frac{1}{3}, \end{aligned}$$

and the values for α_i and β_{ij} are retrieved from a Butcher tableau [30].

The Störmer-Verlet discretisation method is, next to the Runge-Kutta method, one of the most widely known discretisation techniques in the field of engineering [31]. The method uses a Taylor approximation and central differences formulation to discretise a second order differential equation. As an example, a system

$$\begin{aligned} \ddot{x} &= f(x,t), \\ x(t_0) &= x_0, \end{aligned} \tag{2.9}$$

is solved using the approximation

$$\ddot{x}(t) \approx \frac{x_{i+1} - 2x_i + x_{i-1}}{\Delta t^2} \tag{2.10}$$

and an appropriate initial condition related to velocity.

In the next chapter, the building blocks of the mimetic spectral element technique are discussed and the procedure for time-dependent energy conserving spectral element schemes is derived.

3 Mathematical background

This chapter focuses on the mathematical background of the mimetic spectral element method. As the equations of motion are derived from Lagrangian and Hamiltonian mechanics, these two concepts are treated in Section 3.1, followed by an explanation of variational analysis in Section 3.2. The derivation for exact energy behaviour at continuous level is treated in Section 3.3. Before diving into the basics of the mimetic spectral element method, coordinate transformation of the time variable is treated in Section 3.4.

The elementary building blocks of the mimetic spectral element methods are treated in Sections 3.6 to 3.8.

There is different notation used in this chapter, among them are not only the continuous and discrete equations, but also vector and matrix notations. To distinguish between the aforementioned, the different notation is hence used. The explanation of all variables is given in the nomenclature at the beginning of this thesis.

3.1 Lagrangian and Hamiltonian mechanics

Classical Newtonian mechanics can be seen as the all-round mechanical system that is used in everyday life. From a historical point of view it brought people great achievements. The equations of motion that define the problem at hand are often related to inertial reference frames and can be traced back to Newton's three laws of motion, i.e. Newton's first, second and third law.

A more general field of studies, Lagrangian mechanics, was founded by Joseph-Louis Lagrange [25]. As a reformulation of classical Newtonian mechanics, Lagrangian mechanics is a more generalised formulation that can be best described by the two principles

- that a state of a mechanical system is expressed in minimal coordinates and
- that a mechanical system min- or maximises a so-called action.

Let a Lagrangian be formulated as

$$L(x(t), \dot{x}(t), t) = T(\dot{x}(t)) - V(x(t)), \tag{3.1}$$

i.e. the difference between kinetic energy and potential energy of the system. Equation (3.1) is dependent on x and $\dot{x}$ but can also depend on t. The remainder of this section treats the most general version of the Lagrangian.

The Lagrangian equations of motion is found through substituting (3.1) in

$$\frac{\mathrm{d}}{\mathrm{d}t}\left(\frac{\partial L}{\partial \dot{x}}\right) - \frac{\partial L}{\partial x} = 0, \tag{3.2}$$

which is the Euler-Lagrange equation that is derived from the action

$$S(x(t), \dot{x}(t)) = \int_{t_1}^{t_2} \left[L(x(t), \dot{x}(t), t) \right] \, dt, \tag{3.3}$$

by means of variational analysis [24]. Variational analysis is treated more thoroughly in Section 3.2, in which also (3.2) is derived. With the introduction of the conjugate momenta

$$p_k = \frac{\partial L}{\partial \dot{x}_k} \left(x(t), \dot{x}(t), t \right),$$

Hamilton simplified the Lagrangian and defined the Hamiltonian through

$$H(p(t), x(t), t) \equiv \dot{x}(t) \frac{\partial L}{\partial \dot{x}} \left(x(t), \dot{x}(t), t \right) - L \left(x(t), \dot{x}(t), t \right). \tag{3.4}$$

Through the Hamiltonian, (3.2) is written as a first order system like

$$\dot{p} = -\frac{\partial H}{\partial x} \left(p(t), x(t), t \right) \quad \text{and} \quad \dot{x} = \frac{\partial H}{\partial p} \left(p(t), x(t), t \right),$$

defining the equations of motion. For the case that will be treated in Chapter 4, the Hamiltonian can be written as

$$\begin{aligned} H(x(t), \dot{x}, t) &= \dot{x}(t) \frac{\partial L}{\partial \dot{x}} \left(x(t), \dot{x}(t), t \right) - L \left(x(t), \dot{x}(t), t \right), \\ &= \dot{x}(t) \frac{\partial L}{\partial \dot{x}} \left(x(t), \dot{x}(t), t \right) - \left(\frac{1}{2} m \dot{x}^2(t) - \frac{1}{2} k x^2(t) \right), \\ &= \dot{x}(t) m \dot{x}(t) - \left(\frac{1}{2} m \dot{x}^2(t) - \frac{1}{2} k x^2(t) \right), \\ &= \frac{1}{2} m \dot{x}^2(t) + \frac{1}{2} k x^2(t), \end{aligned}$$

where $T(\dot{x}(t)) = \frac{1}{2} m \dot{x}^2(t)$ and $V(x(t)) = \frac{1}{2} k x^2(t)$ are substituted in (3.1). Since the Hamiltonian is defined by position and its conjugate momenta, it is rewritten as

$$H(p(t), x(t), t) = \frac{p^2(t)}{2m} + \frac{1}{2} k x^2(t),$$

defining the total energy of the system.

3.2 Variational analysis and its applications

The main idea behind variational analysis is to find a minimum of some functional by infinitesimally distorting its minimum. Let (3.3) serve as an example. If $S(\hat{x}(t))$ is its minimum at curve $\hat{x}(t)$, it follows that $S(\hat{x}(t) + \alpha \delta x(t)) \geq S(\hat{x}(t))$. Here $\delta x(t)$ is considered a perturbation in any direction in space. From minimisation procedures it is known that a minimum (or maximum)

is found when its first derivative is 0 for all perturbations $\delta x(t)$ or

$$\begin{aligned} 0 &= \frac{\mathrm{d}}{\mathrm{d}\alpha} S(\hat{x}(t) + \alpha\delta x(t))\bigg|_{\alpha=0}, \\ &= \int_{t_1}^{t_2} \left[\frac{\mathrm{d}}{\mathrm{d}\alpha} L(\hat{x}(t) + \alpha\delta x(t), \dot{\hat{x}}(t) + \alpha\delta\dot{x}(t), t)\bigg|_{\alpha=0} \right] dt, \\ &= \int_{t_1}^{t_2} \left[\frac{\partial L}{\partial x}\frac{\mathrm{d}x}{\mathrm{d}\alpha} + \frac{\partial L}{\partial \dot{x}}\frac{\mathrm{d}\dot{x}}{\mathrm{d}\alpha} \right]_{\alpha=0} dt, \\ &= \int_{t_1}^{t_2} \left[\frac{\partial L}{\partial x}\delta x + \frac{\partial L}{\partial \dot{x}}\delta\dot{x} \right]_{\alpha=0} dt. \end{aligned} \tag{3.5}$$

Note that $x(t) = \hat{x}(t) + \alpha\delta x(t)$ and $\dot{x}(t) = \dot{\hat{x}}(t) + \alpha\delta\dot{x}(t)$ were used. Furthermore, rewriting $\delta\dot{x}(t) = \frac{\mathrm{d}}{\mathrm{d}t}\delta x(t)$ enables it to write (3.5) as

$$\begin{aligned} 0 &= \int_{t_1}^{t_2} \left[\frac{\partial L}{\partial x}\delta x(t) + \frac{\partial L}{\partial \dot{x}}\frac{\mathrm{d}}{\mathrm{d}t}\delta x(t) \right]_{\alpha=0} dt, \\ &= \int_{t_1}^{t_2} \left[\frac{\partial L}{\partial x}\delta x(t) - \frac{\mathrm{d}}{\mathrm{d}t}\left(\frac{\partial L}{\partial \dot{x}}\right)\delta x(t) \right]_{\alpha=0} dt + \delta x(t)\frac{\partial L}{\partial \dot{x}}\bigg|_{t_1}^{t_2}, \\ &= \int_{t_1}^{t_2} \left[\frac{\partial L}{\partial x} - \frac{\mathrm{d}}{\mathrm{d}t}\left(\frac{\partial L}{\partial \dot{x}}\right) \right]_{\alpha=0} \delta x(t)\, dt. \end{aligned} \tag{3.6}$$

To go from the penultimate phrasing to the last required no end point variations, i.e. $\delta x(t_1) = \delta x(t_2) = 0$. This is the case when then end points $x(t_1)$ and $x(t_2)$ are fixed. For (3.6) to be 0 for all possible variations $\delta x(t)$ finally results in

$$\frac{\mathrm{d}}{\mathrm{d}t}\left(\frac{\partial L}{\partial \dot{x}}\right) - \frac{\partial L}{\partial x} = 0 \quad \forall t \in [t_1, t_2]\,. \tag{3.7}$$

Note that (3.2), the Euler-Lagrange equation has been derived [24].

3.3 Energy conservation and Noether's theorem

Another interesting aspect regarding the Lagrangian formulation was found by Amalie Emmy Noether. In 1918 it was stated that with every invariant of the Lagrangian a conservation law was related [24, p. 55]. Relating this to the common thread of this work means that whenever time invariance is found, total energy is conserved.

Once again, let $L(x, \dot{x}, t)$ be the general expression of the Lagrangian. In the subsequent paragraphs, using the procedure of variational analysis, a formulation for energy conservation

is found. Variational analysis of the Lagrangian is written as

$$\begin{aligned}\delta L(x,\dot{x},t) &= \frac{\mathrm{d}}{\mathrm{d}\alpha}L(\hat{x}+\alpha\delta x,\dot{\hat{x}}+\alpha\delta\dot{x},t)\bigg|_{\alpha=0}, \\ &= \left[\frac{\partial L}{\partial x}\frac{\mathrm{d}x}{\mathrm{d}\alpha}+\frac{\partial L}{\partial \dot{x}}\frac{\mathrm{d}\dot{x}}{\mathrm{d}\alpha}\right]\bigg|_{\alpha=0}, \\ &= \delta x\left[\frac{\partial L}{\partial x}-\frac{\mathrm{d}}{\mathrm{d}t}\left(\frac{\partial L}{\partial \dot{x}}\right)\right]+\frac{\mathrm{d}}{\mathrm{d}t}\left(\delta x\frac{\partial L}{\partial \dot{x}}\right),\end{aligned} \tag{3.8}$$

where the product rule of differentiation is used in the last rewriting of the equation [24]. The first expression on the right-hand side is known as the Euler-Lagrange equation as described in Section 3.2 and equals zero if and only if the equations of motion are obeyed. Variational analysis of the Lagrangian can hence be written as

$$\delta L(x(t),\dot{x}(t),t) = \frac{\mathrm{d}}{\mathrm{d}t}\left(\delta x(t)\frac{\partial L}{\partial \dot{x}}\left(x(t),\dot{x}(t),t\right)\right). \tag{3.9}$$

From another perspective, as t is the only independent variable, time-like variations of the Lagrangian results in

$$\begin{aligned}0 &= \delta\int_{t_1}^{t_2}[L]\;dt, \\ &= \int_{t_1}^{t_2}\left[\delta L+\delta t\frac{\partial L}{\partial t}\right]\;dt+\int_{t_1}^{t_2}L\,d\delta t, \\ &= \int_{t_1}^{t_2}\left[\delta L+\delta t\frac{\partial L}{\partial t}\right]\;dt-\int_{t_1}^{t_2}\delta t\,dL+L\delta t\bigg|_{t_1}^{t_2}, \\ &= \int_{t_1}^{t_2}\left[\delta L-\delta t\left(\frac{\mathrm{d}L}{\mathrm{d}t}-\frac{\partial L}{\partial t}\right)\right]\;dt,\end{aligned} \tag{3.10}$$

in which no end point variations were allowed [24]. For (3.10) to be 0 it follows that

$$\delta L(x(t),\dot{x}(t),t) = \delta t\left(\frac{\mathrm{d}L}{\mathrm{d}t}-\frac{\partial L}{\partial t}\right). \tag{3.11}$$

At this moment there are two expressions ((3.9) and (3.11)) to the same variation of the Lagrangian. Setting both to be equal to each other and rewriting the resulting expression leads to

$$\begin{aligned}\frac{\mathrm{d}}{\mathrm{d}t}\left(\delta x\frac{\partial L}{\partial \dot{x}}\right) &= \delta t\left(\frac{\mathrm{d}L}{\mathrm{d}t}-\frac{\partial L}{\partial t}\right), \\ \delta t\frac{\mathrm{d}}{\mathrm{d}t}\left(\dot{x}\frac{\partial L}{\partial \dot{x}}\right) &= \delta t\left(\frac{\mathrm{d}L}{\mathrm{d}t}-\frac{\partial L}{\partial t}\right), \\ \frac{\mathrm{d}}{\mathrm{d}t}\left(\dot{x}\frac{\partial L}{\partial \dot{x}}-L\right) &= -\frac{\partial L}{\partial t},\end{aligned} \tag{3.12}$$

in which the expression $\delta x = \dot{x}\delta t$ is used to proceed from the first line to the second [24]. Equation (3.12) is known as Euler's second equation for the Lagrangian and becomes an energy

conservation equation when the Lagrangian is explicitly independent of time, i.e. the right-hand side equals zero. The same result can also be obtained considering the derivative of $L(x(t), \dot{x}(t), t)$ with respect to t. This is done through

$$\begin{aligned}
\frac{\mathrm{d}L}{\mathrm{d}t} &= \frac{\partial L}{\partial t} + \frac{\partial L}{\partial x}\frac{\mathrm{d}x}{\mathrm{d}t} + \frac{\partial L}{\partial \dot{x}}\frac{\mathrm{d}\dot{x}}{\mathrm{d}t}, \\
&= \frac{\partial L}{\partial t} + \frac{\partial L}{\partial x}\frac{\mathrm{d}x}{\mathrm{d}t} + \frac{\mathrm{d}}{\mathrm{d}t}\left(\frac{\partial L}{\partial \dot{x}}\dot{x}\right) - \frac{\mathrm{d}}{\mathrm{d}t}\left(\frac{\partial L}{\partial \dot{x}}\right)\frac{\mathrm{d}x}{\mathrm{d}t}, \\
&= \frac{\partial L}{\partial t}\left(\frac{\partial L}{\partial x} - \frac{\mathrm{d}}{\mathrm{d}t}\left(\frac{\partial L}{\partial \dot{x}}\right)\right)\frac{\mathrm{d}x}{\mathrm{d}t} + \frac{\mathrm{d}}{\mathrm{d}t}\left(\frac{\partial L}{\partial \dot{x}}\dot{x}\right), \\
\frac{\partial L}{\partial t} &= \frac{\mathrm{d}}{\mathrm{d}t}\left(L - \frac{\partial L}{\partial \dot{x}}\dot{x}\right),
\end{aligned}$$

in which the Euler-Lagrange equation is used to go from the penultimate expression to the last. In other words, the Lagrangian is time invariant if and only if

$$\frac{\partial L}{\partial t} = 0, \tag{3.13}$$

meaning that the Lagrangian does not explicitly depend on time. If and only if this is the case, then energy is conserved. Equation (3.13) will be used later on in Chapter 4 to assess energy behaviour. The Hamiltonian, (3.4), may be recognised in (3.13). Substituting the Lagrangian

$$L(x(t), \dot{x}(t), t) = \frac{1}{2}m\dot{x}^2(t) - \frac{1}{2}kx^2(t), \tag{3.14}$$

into (3.13), it follows that the energy of the system is conserved through

$$\begin{aligned}
\frac{\mathrm{d}}{\mathrm{d}t}\left(\dot{x}\frac{\partial L}{\partial \dot{x}} - L\right) &= \frac{\mathrm{d}}{\mathrm{d}t}\left(\dot{x}(t)m\dot{x}(t) - \left(\frac{1}{2}m\dot{x}^2(t) - \frac{1}{2}kx^2(t)\right)\right), \\
&= \frac{\mathrm{d}}{\mathrm{d}t}\left(\frac{1}{2}m\dot{x}^2(t) + \frac{1}{2}kx^2(t)\right), \\
&= 0,
\end{aligned} \tag{3.15}$$

which indicates that $L(x(t), \dot{x}(t), t)$ from (3.14) is invariant under time translations.

3.4 Coordinate transformation of the time variable

A time-line may be solved directly or a time-line may be split up into a distinct amount of sections, after which each section is solved separately. The latter is known as h-convergence. Let $[a, b]$ in Figure 3.1 be an arbitrary time interval and let this time interval be one of the distinct sections. Mapping this interval onto the reference interval $\tau \in [-1, 1]$ can most easily be done using linear interpolation, i.e. through

$$\tau(t) = 2\frac{(t-a)}{b-a} - 1, \tag{3.16}$$

or vice versa

$$t(\tau) = \frac{b-a}{2}(\tau + 1) + a. \tag{3.17}$$

Equations (3.16) and (3.17) are used in Section 4.3, where a known mapping is used. Section 4.4 deals with an arbitrary mapping and arbitrary $\frac{\mathrm{d}t}{\mathrm{d}\tau}(t)$. These two sections will be compared to each other.

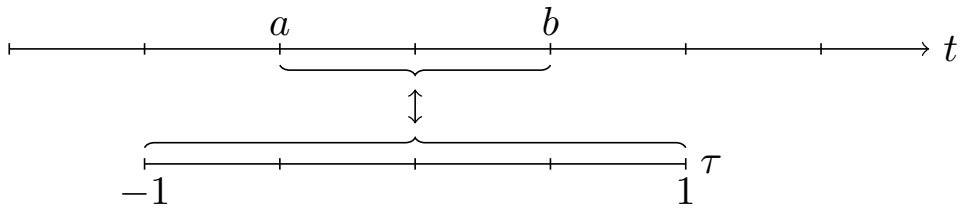

Figure 3.1: Coordinate transformation of an arbitrary time interval $t \in [a, b]$ to $\tau \in [-1, 1]$.

3.5 Intermediate summary

All mathematics that was treated in Sections 3.1 to 3.4 dealt with mathematics at a continuous level. Since continuous domains cannot be solved using computer software, these need to be transformed to discrete variables. All subsequent sections that follow deal with discrete mathematics. It is therefore sensible to put the continuous mathematics in sequence. This is done in Figure 3.2. The penultimate block in Figure 3.2 results in the equations of motion of the system, known as the Euler-Lagrange equations. Knowing this equation, energy conservation can be derived at continuous level.

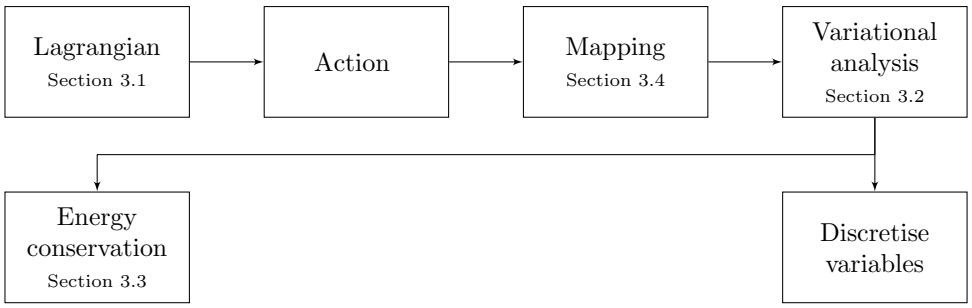

Figure 3.2: Block diagram showing the procedure at continuous level.

The subsequent sections elaborate on the basis functions (Section 3.6), the primal grid and its invisible dual grid (Section 3.7) and the incidence matrices (Section 3.8) that allow for the conversion between nodal and edge functions.

3.6 One- and two-dimensional primal basis functions

The mimetic spectral element technique uses the Legendre-Gauss-Lobatto nodes and Lagrange polynomials $l_i(\tau)$ to discretise the continuous quantities. The Legendre-Gauss-Lobatto nodes, τ_i, more thoroughly explained in [32], are all $p + 1$ root locations of the polynomial

$$f(\tau) = (1 - \tau^2)\frac{\mathrm{d}L_p(\tau)}{\mathrm{d}\tau}. \tag{3.18}$$

The $p+1$ root locations have a symmetric layout on the domain $\tau \in [-1, 1]$ and are depicted in Figure 3.3. The Legendre-Gauss-Lobatto nodes are symmetric around $\tau = 0$. The Legendre polynomials are defined through

$$L_i(\tau) = \frac{1}{2^i i!}\frac{\mathrm{d}^i}{\mathrm{d}\tau^i}\left(\tau^2 - 1\right)^i, \quad i = 0, 1, \ldots, p, \tag{3.19}$$

indicating, among others, that $L_0 = 1$ and $L_1 = \tau$. Reducing the Lagrange polynomials $l_i(\tau)$ leads to a special property, dictating

$$\mathcal{R}l_i^0(\tau) = l_i^0(\tau_p) = h_i(\tau) = \begin{cases} 1 & \text{for} \quad i = p \\ 0 & \text{for} \quad i \neq p \end{cases} . \tag{3.20}$$

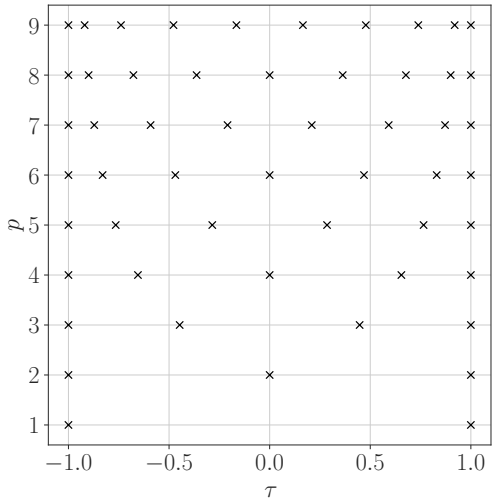

Figure 3.3: $p + 1$ root locations of (3.18) using (3.19) for different p on $\tau \in [-1, 1]$.

The property mentioned in (3.20) enables it to discretise 0-forms (related to nodal points) as Lagrange polynomials are 0-forms as well. Through

$$\pi_h a^0(\tau) = \sum_{i=0}^{p} a_i h_i(\tau), \tag{3.21}$$

the definition of the nodal basis function is created. The nodal basis functions for $p = 3$ are plotted in Figure 3.4a. Edge basis functions are derived from nodal basis functions through

$$e_j(\tau) = -\sum_{i=0}^{j-1} dh_i(\tau), \tag{3.22}$$

as proved in [33]. The edge basis functions encompass the property that the integral quantity

$$\int_{\tau_{i-1}}^{\tau_i} [e_j(\tau)] \, d\tau = \begin{cases} 1 & \text{for} \quad i = j \\ 0 & \text{for} \quad i \neq j \end{cases} . \tag{3.23}$$

The primal edge basis functions are shown in Figure 3.4b for $p = 3$. The choice of primal and dual nodes is explained in Section 3.7. The extension to multidimensional domains, like space-time is easily done by means of the tensor product [34]. Using (3.22), 1-forms are discretised as

$$\pi_h a^1(\tau) = \sum_{i=1}^{p} a_i e_i(\tau), \tag{3.24}$$

in which

$$a_i = \int_{\tau_{i-1}}^{\tau_i} a^1 \, d\tau. \tag{3.25}$$

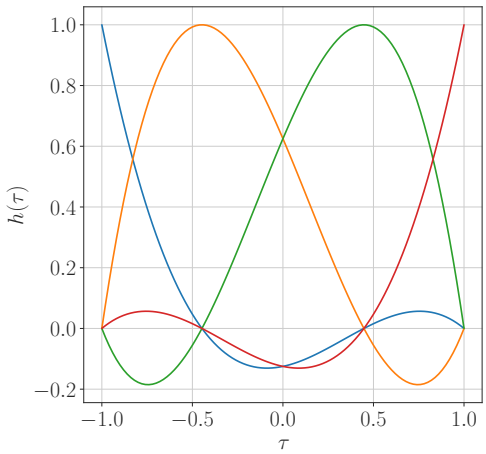

(a) Nodal basis functions for $p = 3$ on the primal grid.

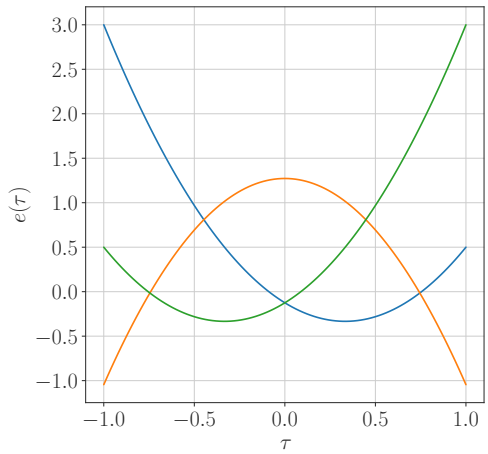

(b) Nodal edge functions for $p = 3$ on the primal grid.

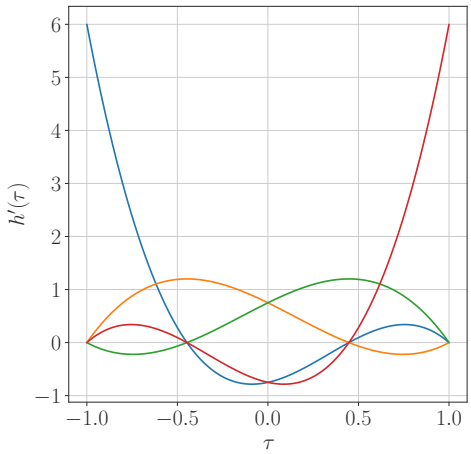

(c) Nodal basis functions for $p = 3$ on the dual grid.

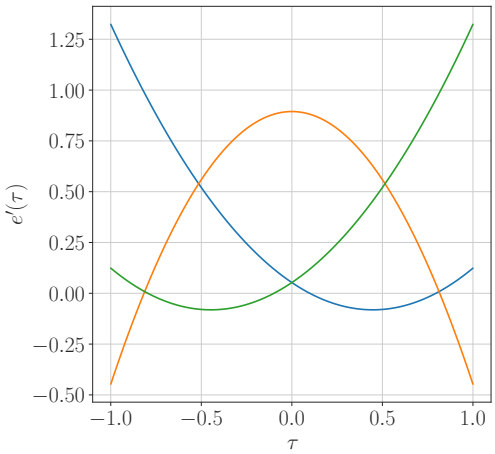

(d) Nodal edge functions for $p = 3$ on the dual grid.

Figure 3.4: Primal and dual basis functions for $p = 3$.

3.7 Primal and dual grid construction

As indicated by Figure 3.3, the polynomial degree p defines the gridpoints. Let for instance $p = 2$. The corresponding grid is shown in Figure 3.5. For clarity the dual space is also given. The dual space follows from the choice of primal basis. By limiting the basis to a canonical

basis, this means that

$$\int_{-1}^{1} \left[\bar{\mathcal{H}}^T \tilde{\mathcal{H}}\right] \, dt = \mathbb{I}, \tag{3.26}$$

and

$$\int_{-1}^{1} \left[\bar{\mathcal{E}}^T \tilde{\mathcal{E}}\right] \, dt = \mathbb{I}, \tag{3.27}$$

in which the vectors of basis functions $\mathcal{H} = [h_0(\tau), \cdots, h_p(\tau)]$ and $\mathcal{E} = [e_1(\tau), \cdots e_p(\tau)]$ have been introduced. In [34] a more thorough derivation is found constituting the dual basis. In short, the exact locations of the dual nodes are unknown, but are computed using

$$\tilde{\mathcal{H}}^T = \bar{\mathcal{H}}^T \left(\mathbb{M}^0\right)^{-1}, \tag{3.28}$$

as explained in [34]. $\mathbb{M}^0$ is shorthand notation for

$$\mathbb{M}^0 = \int_{-1}^{1} \left[\bar{\mathcal{H}}^T \bar{\mathcal{H}}\right] \, dt. \tag{3.29}$$

In a similar fashion, the dual edge basis functions are constructed. This is done through

$$\tilde{\mathcal{E}}^T = \bar{\mathcal{E}}^T \left(\mathbb{M}^1\right)^{-1}, \tag{3.30}$$

where

$$\mathbb{M}^1 = \int_{-1}^{1} \bar{\mathcal{E}}^T \bar{\mathcal{E}} \, dt. \tag{3.31}$$

The use of both the primal and dual basis functions results in a sparse matrix that contains sub-matrices containing the entries 0, 1 and -1. These sub-matrices are called incidence matrices and will be addressed in Section 3.8. The nodal and edge basis functions on the dual grid are shown in Figures 3.4c and 3.4d.

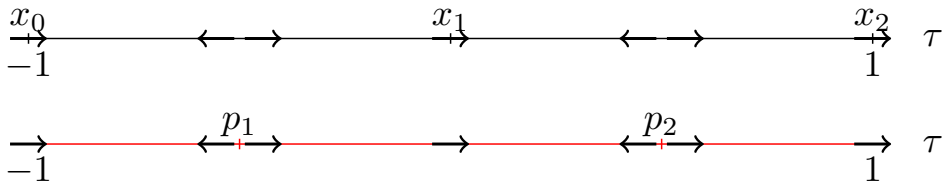

Figure 3.5: One-dimensional primal and dual grid for $p = 2$. Arrows indicate default positive orientation.

3.8 Incidence matrices

Derived from (3.22), derivatives of 0-forms include incidence matrices, i.e. the relation between 0-forms and 1-forms. From (3.22) it follows that [33, 34]

$$\frac{\mathrm{d}h_j}{\mathrm{d}\tau} = e_j(\tau) - e_{j+1}(\tau). \tag{3.32}$$

Relating this to our 0-forms, its derivative is thus

$$\begin{aligned} d\pi_h a^0(\tau) &= d\sum_{i=0}^{p} a_i h_i(\tau), \\ &= \sum_{i=0}^{p} a_i dh_i(\tau), \\ &= \sum_{i=0}^{p} a_i \left(e_i(\tau) - e_{i+1}(\tau)\right), \\ &= \sum_{i=1}^{p} \left(a_i - a_{i-1}\right) e_i(\tau). \end{aligned} \tag{3.33}$$

Transforming (3.33) to vector calculus results in the establishment of the incidence matrix through

$$d\pi_h a^0(\tau) = \bar{\mathbb{E}}^{(1,0)} \vec{\bar{a}} \vec{\bar{e}}. \tag{3.34}$$

The same derivation can be followed for the incidence matrix on the dual grid, $\tilde{\mathbb{E}}^{(1,0)}$. Using the chosen orientation as shown in Figure 3.5 however, $\tilde{\mathbb{E}}^{(1,0)}$ and $\bar{\mathbb{E}}^{(1,0)}$ are related through

$$\tilde{\mathbb{E}}^{(1,0)} = \bar{\mathbb{E}}^{(1,0)^T}. \tag{3.35}$$

Using the theory described above, the incidence matrix related to the primal grid reads

$$\begin{bmatrix} -1 & 1 & 0 & \cdots & 0 \\ 0 & -1 & 1 & \ddots & \vdots \\ \vdots & \ddots & \ddots & \ddots & 0 \\ 0 & \cdots & 0 & -1 & 1 \end{bmatrix}. \tag{3.36}$$

Similarly, the incidence matrix related to the dual grid reads

$$\begin{bmatrix} -1 & 0 & \cdots & 0 \\ 1 & -1 & \ddots & \vdots \\ 0 & 1 & \ddots & 0 \\ \vdots & \ddots & \ddots & -1 \\ 0 & \dots & 0 & 1 \end{bmatrix}. \tag{3.37}$$

3.9 Summary

This chapter is concluded with a summary about the mimetic spectral element discretisation method. In Section 3.5 the procedure at continuous level was already discussed. This section

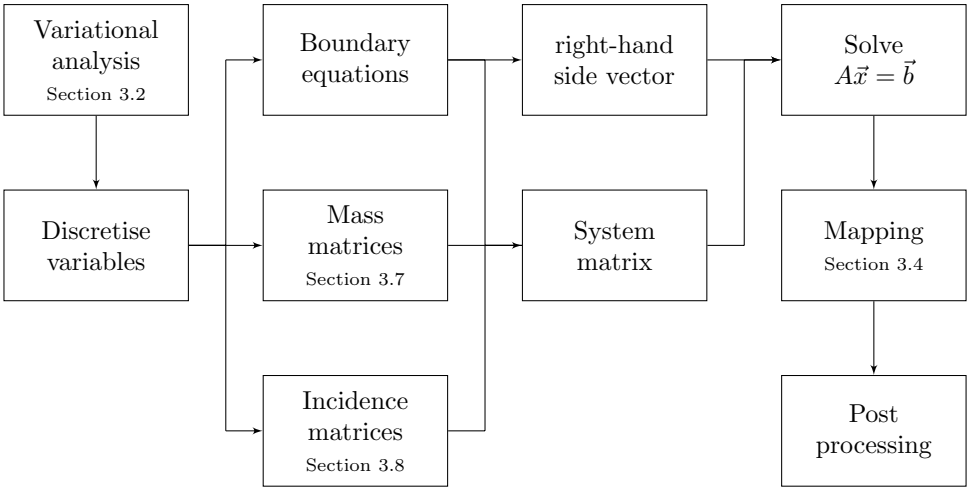

Figure 3.6: Block diagram showing the procedure at discrete level.

elaborates upon the procedure at discrete level. In Figure 3.6 the discrete procedure is shown. The block at the top-right corner solves for the degrees of freedom at both the primal grid and dual grid. Through post processing, visualisation and error computation is performed.

It is found that the discretisation was solely dependent on the construction of the primal grid, i.e. the dual grid is entirely dependent on the primal grid.

Moreover, it was is found that the derivative with respect to time can be exactly represented by the incidence matrix $\bar{\mathbb{E}}$ on the primal grid and $\bar{\mathbb{E}}$ on the dual grid.

4 Simple harmonic oscillator

The simple harmonic oscillator mainly serves as a sample problem for ordinary differential equations in university text books. Either with or without damping it is an understandable phenomenon that can be encountered in everyday life. Recall for instance the swing example in Chapter 1. Because of this relatability, it is also regarded as a meaningful starting point for the new time-dependent mimetic spectral element technique. This chapter commences with the problem statement and the continuous solution to the simple harmonic oscillator in Section 4.1. A discrete Lagrangian and its variational integrator technique are treated in Section 4.2 and a first starting point towards mimetic spectral elements for time-dependent problems is treated in Section 4.3. A slightly more sophisticated approach is considered in Section 4.4 and a spectral marching method is explained and tested in Section 4.5.Everything is summarised in Section 4.6.

4.1 Problem statement

Let the problem be defined as follows. Let there be a concentrated mass m at one end of a spring with spring constant k. Furthermore, let the other side of the spring be attached to an immovable wall, as shown in Figure 4.1. This problem is known as the simple harmonic oscillator. The well known equation of motion for this equation of motion reads

$$m\ddot{x}(t) + kx(t) = 0. \tag{4.1}$$

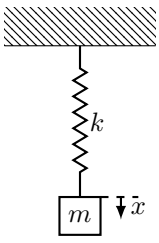

Figure 4.1: Undamped mass spring system.

Equation (4.1) is a second order ordinary differential equation and integrating twice requires two initial conditions $x(0)$ and $\dot{x}(0)$. The well-posed problem that is being treated in this chapter is to find $x(t)$ such that

$$
\begin{aligned}
m\ddot{x}(t) + kx(t) &= 0, \\
x(0) &= A \quad \text{and} \\
\dot{x}(0) &= B, \quad \text{with} \\
A &= 1, \\
B &= 0, \\
m &= 5 \quad \text{and} \\
k &= 1.
\end{aligned}
$$

The general solution to (4.1) can be found by assuming

$$x(t) = e^{rt}.$$

Differentiating twice with respect to variable t and applying the initial conditions $x(0)$ and $\dot{x}(0)$ eventually results in the continuous solution

$$x(t) = A\cos\left(\sqrt{\frac{k}{m}}t\right). \tag{4.2}$$

The full derivation can be found in Appendix A. Equation (4.2) is plotted in Figure 4.2a. Figure 4.2b shows momentum, defined as

$$
\begin{aligned}
p(t) &= m\dot{x}(t) \\
&= -A\sqrt{km}\sin\left(\sqrt{\frac{k}{m}}t\right).
\end{aligned} \tag{4.3}
$$

Total energy at each timestep is given by

$$
\begin{aligned}
E(t) &= \frac{1}{2}m\dot{x}^2(t) + \frac{1}{2}kx^2(t), \\
&= \frac{1}{2}mA^2\left(-\sqrt{\frac{k}{m}}\sin\left(\sqrt{\frac{k}{m}}t\right)\right)^2 + \frac{A^2}{2}k\left(\cos\left(\sqrt{\frac{k}{m}}t\right)\right)^2, \\
&= \frac{1}{2}kA^2,
\end{aligned} \tag{4.4}
$$

and shown in Figure 4.2c. Figure 4.2d shows the exact position-momentum plot, which over time should not spiral in- or outwards. In the subsequent sections, the exact solutions of position, momentum and energy are plotted as a reference.

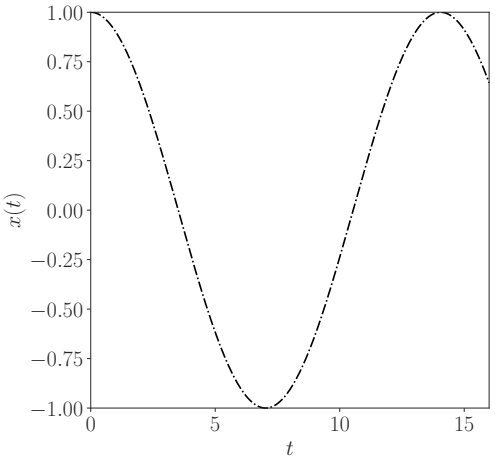

(a) Position

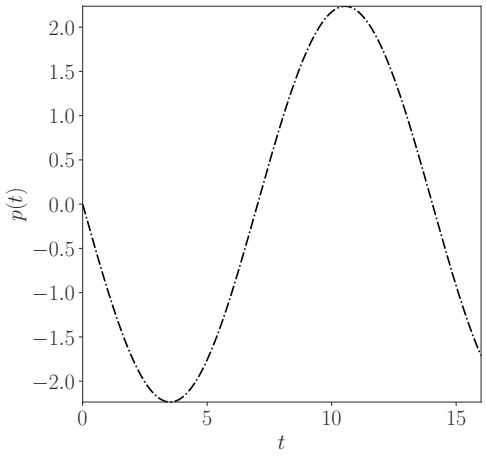

(b) Momentum

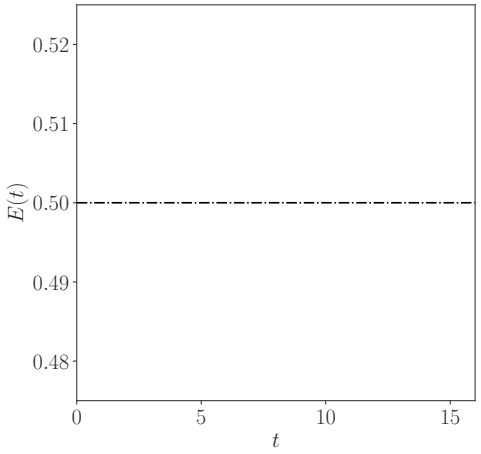

(c) Energy

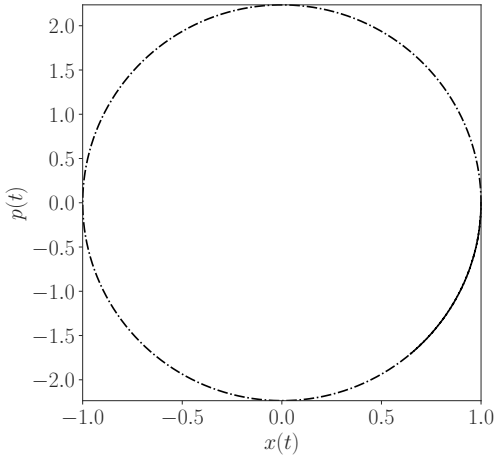

(d) Position - momentum

Figure 4.2: Exact solution $(- \cdot -)$ to (4.1) using (4.2) to (4.4).

4.2 Discretising using the variational integrator technique

Let the variational integrator technique be the first technique to be considered that tries to capture all relevant physics. Equation (4.1) can be discretised straighforwardly using a Taylor series around $x(t)$. This section however, takes a different route by looking at the related discrete Lagrangian $L_d(x_0, x_1, \Delta t)$ and continues from there. A block diagram is found in Figure 4.3. Let the continuous and discrete Lagrangian be defined in (4.5) and (4.6) as

$$\begin{aligned} L(x(t), \dot{x}(t), t) &= \int_a^b \left[T(\dot{x}(t)) - V(x(t))\right] \, dt, \\ &= \int_a^b \left[\frac{1}{2} m \dot{x}^2(t) - \frac{1}{2} k x^2(t)\right] \, dt \end{aligned} \tag{4.5}$$

and

$$L_d(x_0, x_1, \Delta t) = \Delta t \left[\frac{1}{2} \left(\frac{x_1 - x_0}{\Delta t} \right)^T \mathbb{M} \left(\frac{x_1 - x_0}{\Delta t} \right) - \frac{1}{2} x_0^T \mathbb{K} x_0 \right], \tag{4.6}$$

where [24]

$$L_d(x_0, x_1, \Delta t) \approx \int_{x_0}^{x_1} L(x(t), \dot{x}(t), t)\, dt.$$

$\mathbb{M}$ and $\mathbb{K}$ are diagonal matrices containing m and k on their diagonal as

$$\mathbb{M} = \begin{bmatrix} m & 0 & \cdots & 0 \\ 0 & \ddots & \ddots & \vdots \\ \vdots & \ddots & \ddots & 0 \\ 0 & \cdots & 0 & m \end{bmatrix} \quad \text{and} \quad \mathbb{K} = \begin{bmatrix} k & 0 & \cdots & 0 \\ 0 & \ddots & \ddots & \vdots \\ \vdots & \ddots & \ddots & 0 \\ 0 & \cdots & 0 & k \end{bmatrix}.$$

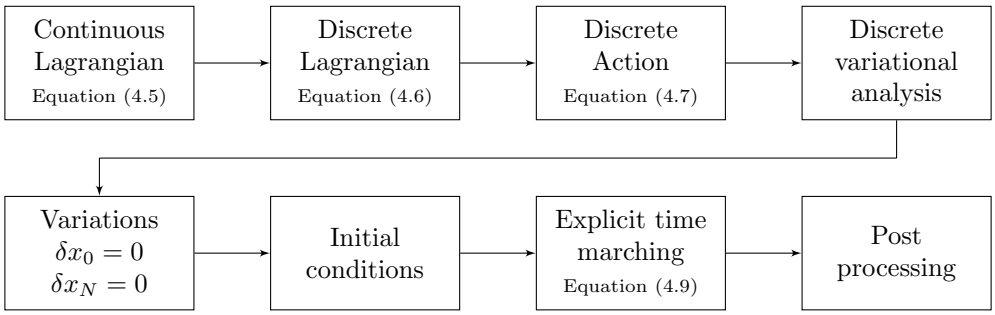

Figure 4.3: Block diagram showing the variational integrator technique.

The derivative $\dot{x}(t)$ is approximated by a first order accurate Taylor series. The discrete action of (4.6) is a summation over the domain. Requiring this action to be stationary results in

$$\begin{aligned}
0 &= \delta \sum_{i=0}^{N-1} \left(\Delta t \left[\frac{1}{2} \left(\frac{x_{i+1} - x_i}{\Delta t} \right)^T \mathbb{M} \left(\frac{x_{i+1} - x_i}{\Delta t} \right) - \frac{1}{2} x_i^T \mathbb{K} x_i \right] \right), \\
&= \sum_{i=0}^{N-1} \delta \left(\Delta t \left[\frac{1}{2} \left(\frac{x_{i+1} - x_i}{\Delta t} \right)^T \mathbb{M} \left(\frac{x_{i+1} - x_i}{\Delta t} \right) - \frac{1}{2} x_i^T \mathbb{K} x_i \right] \right), \\
&= \sum_{i=0}^{N-1} \left(\left[-\mathbb{M} \left(\frac{x_{i+1} - x_i}{\Delta t} \right) - \Delta t \mathbb{K} x_i \right] \cdot \delta x_i + \left[\mathbb{M} \left(\frac{x_{i+1} - x_i}{\Delta t} \right) \right] \cdot \delta x_{i+1} \right) \quad \forall \delta x_i \\
&= \sum_{i=1}^{N-1} \left(\left[-\mathbb{M} \left(\frac{x_{i+1} - x_i}{\Delta t} \right) - \Delta t \mathbb{K} x_i + \mathbb{M} \left(\frac{x_i - x_{i-1}}{\Delta t} \right) \right] \cdot \delta x_i \right) \\
&\quad + \left[-\mathbb{M} \left(\frac{x_1 - x_0}{\Delta t} \right) - \Delta t \mathbb{K} x_0 \right] \cdot \delta x_0 + \left[\mathbb{M} \left(\frac{x_N - x_{N-1}}{\Delta t} \right) \right] \cdot \delta x_N \quad \forall \delta x_i.
\end{aligned} \tag{4.7}$$

Forcing $\delta x_0 = \delta x_N = 0$ results in

$$\begin{aligned}
0 &= -\mathbb{M} \left(\frac{x_{i+1} - x_i}{\Delta t} \right) - \Delta t \mathbb{K} x_i + \mathbb{M} \left(\frac{x_i - x_{i-1}}{\Delta t} \right), \\
&= \mathbb{M} \left(\frac{x_{i+1} - 2x_i + x_{i-1}}{\Delta t^2} \right) + \mathbb{K} x_i.
\end{aligned} \tag{4.8}$$

Equation (4.8) is widely known as a discrete representation of the harmonic oscillator. For $\mathbb{M} = m\mathbb{I}$ and $\mathbb{K} = k\mathbb{I}$ this system enables explicit time marching through

$$\begin{aligned} x_{i+1} &= \left(2 - \frac{k}{m}\Delta t^2\right) x_i - x_{i-1}, \\ &= x_i - x_{i-1} + \left(1 - \frac{k}{m}\Delta t^2\right) x_i, \end{aligned}$$

if the first two positions are known. It is however uncommon to specify two subsequent positions x_0 and x_1, rather an initial position x_0 and initial velocity $\dot{x}_0$. This is done through a first order accurate Taylor series. The resulting solution for position is

$$x_{i+1} = \begin{cases} \left(1 - \frac{k}{m}\Delta t^2\right) x_i + \dot{x}(0)\Delta t & \text{for} \quad i = 0 \\ \left(2 - \frac{k}{m}\Delta t^2\right) x_i - x_{i-1} & \text{for} \quad i > 0 \end{cases} . \tag{4.9}$$

Similar to (4.3), discrete momentum is defined as a multiplication of velocity at time instant i, $\dot{x}_i$ and mass m through

$$\begin{aligned} p_i &= m\dot{x}_i, \\ &= m\frac{x_{i+1} - x_i}{\Delta t}. \end{aligned} \tag{4.10}$$

Equation (4.10) directly follows from (4.9). Discrete total energy at time instant i, E_i is calculated through

$$\begin{aligned} E_i &= \frac{1}{2}\left(\frac{x_{i+1} - x_i}{\Delta t}\right) m \left(\frac{x_{i+1} - x_i}{\Delta t}\right) + \frac{1}{2} x_i k x_i, \\ &= \frac{1}{2}\left(\frac{m}{\Delta t^2}\left(x_{i+1}^2 - 2x_i x_{i+1} + x_i^2\right) + k x_i^2\right), \end{aligned} \tag{4.11}$$

which is not always equal to $\frac{1}{2}kA^2$ (total energy as calculated in (4.4)). Hence, in discrete sense and using the variational integrator technique, energy is not exactly conserved. Figure 4.4 shows the discrete solution using the variational integrator method.

Figure 4.4b shows discrete momentum with respect to discrete time. A striking difference observed from Figure 4.4b is the mismatch in momentum right at $t = 0$. This is a result of the explicit time-marching scheme, i.e. the definition of discrete velocity, $\dot{x}_i = \frac{x_{i+1} - x_i}{\Delta t}$ and recognising that position is first solved for and velocity afterwards. Following, discrete momentum and discrete energy lack one solution at the very last discrete time instant compared to discrete position. This is, once again, a consequence of the definition of discrete velocity.

Figure 4.4c displays discrete energy with respect to discrete time. From Figure 4.4b, it is immediately clear that energy is not exactly conserved. Discrete energy oscillates around the exact energy. The question remains whether the oscillating behaviour damps out, amplifies or is bounded over time. The answer is found in Figure 4.4d.

Figure 4.4d displays, in discrete sense, momentum versus position at multiple time instants. Would energy amplify or decay over time the position momentum plot would spiral out- or inward over time. However, it keeps its circular shape, indicating oscillatory behaviour without damping. This plot is shown for $t \in [0, 1600]$.

The overall conclusion is hence that from this variational integrator perspective, discrete energy is not conserved but oscillates over time. Moreover, discrete velocity and hence discrete momentum, do not obey the continuous initial condition related to velocity. The oscillating behaviour might be addressed to the velocity calculation through the first order accurate Taylor series. As a matter of fact, the velocity calculation is not calculated at point t^i, rather $t^{i+\frac{1}{2}}$.

This means that calculating the energy behaviour of the system always has two components, i.e. potential energy at t^i and kinetic energy at $t^{i+\frac{1}{2}}$. In attempting to solve this issue, another formulation of discrete velocity is used. Using

$$\frac{x_{i+1} - x_{i-1}}{2\Delta t} = \dot{x}_i \tag{4.12}$$

and likewise

$$\frac{x_1 - x_{-1}}{2\Delta t} = \dot{x}(0), \tag{4.13}$$

the solution for position in (4.9) is rewritten to

$$x_{i+1} = \begin{cases} \left(1 - \frac{k}{2m}\Delta t^2\right) x_i + \dot{x}(0)\Delta t & \text{for} \quad i = 0 \\ \left(2 - \frac{k}{m}\Delta t^2\right) x_i - x_{i-1} & \text{for} \quad i > 0 \end{cases} . \tag{4.14}$$

The results are found in Figure 4.5. Position is shown in 4.5a and calculated using (4.14). Using (4.12) and (4.14), momentum is found through

$$p_i = m\frac{x_{i+1} - x_{i-1}}{2\Delta t}, \tag{4.15}$$

of which its result is shown in Figure 4.5b. Energy is shown in Figure 4.5c and calculated through

$$E_i = \frac{1}{2}\left(\frac{x_{i+1} - x_{i-1}}{2\Delta t}\right) m \left(\frac{x_{i+1} - x_{i-1}}{2\Delta t}\right) + \frac{1}{2} x_i k x_i. \tag{4.16}$$

This time, it is shown that both its kinetic energy and potential energy have been used at the same moment t^i. The error between the discrete and the exact solution has decreased significantly in comparison to Figure 4.4c. However, its mean energy has decreased with respect to the former derivation as well. The discrete energy does not oscillate around the exact energy anymore. Only the crests of the discrete energy match the exact energy solution.

Represented by Figure 4.5d, it is indicated by the momentum versus position plot that the system does not damp out nor amplifies. This plot is shown for $t \in [0, 1600]$.

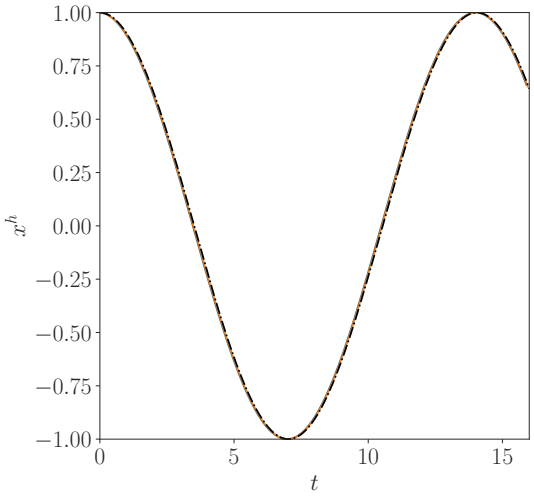

(a) Position

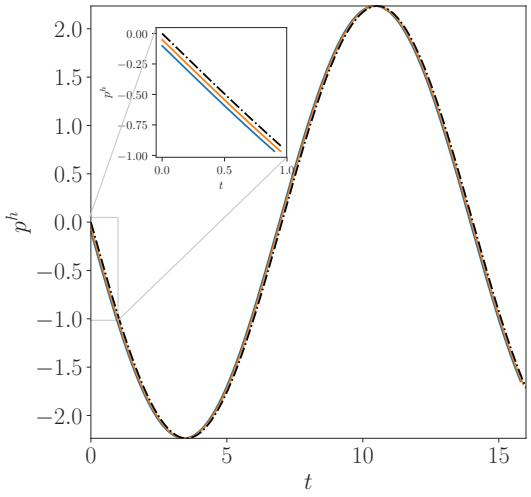

(b) Momentum

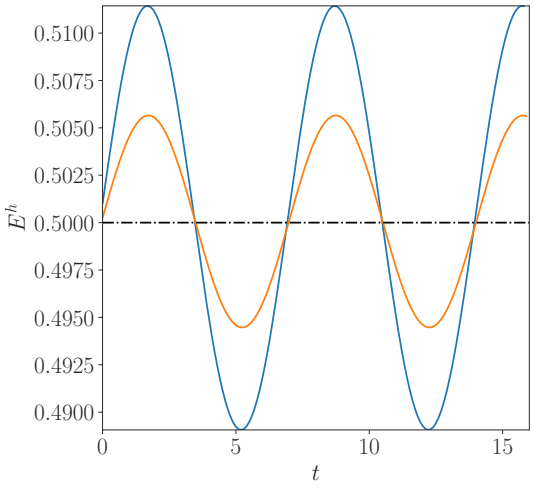

(c) Energy

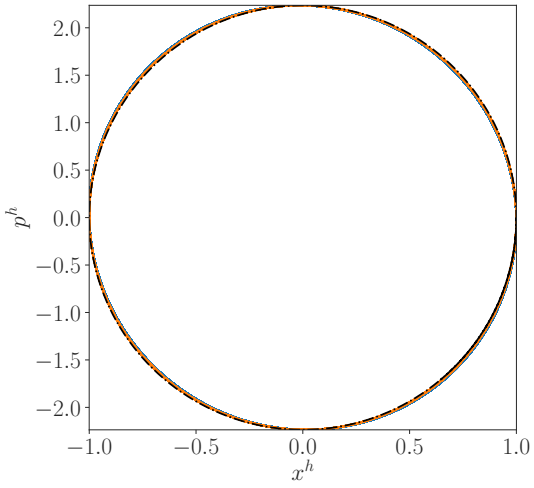

(d) Position - momentum

Figure 4.4: Discrete solution to (4.1) using (4.9) to (4.11). Exact solution shown as $- \cdot -$. Figures 4.4a to 4.4c computed for for $t \in [0, 16]$. Figure 4.4d computed for $t \in [0, 1600]$. $\Delta t = 0.1$ (—), $\Delta t = 0.05$ (—).

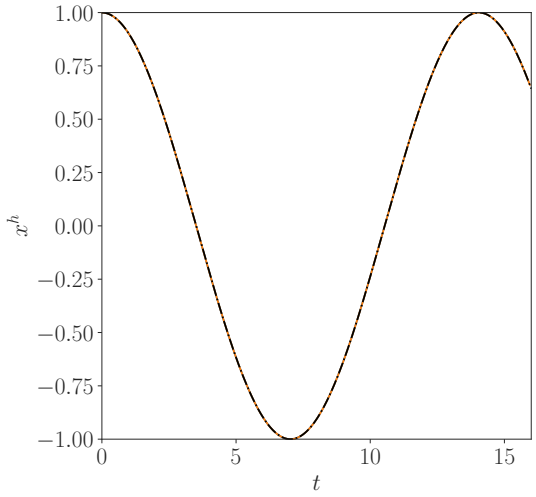

(a) Position

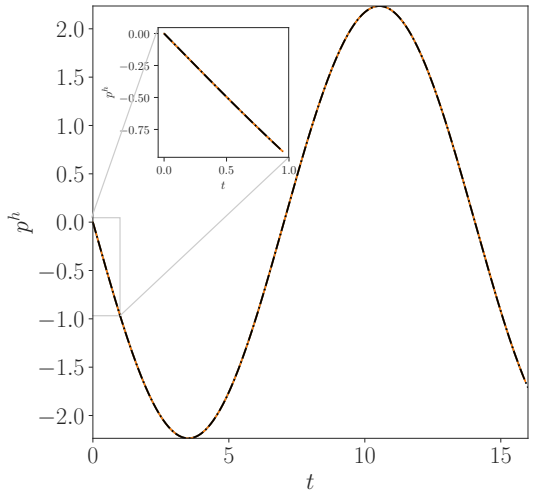

(b) Momentum

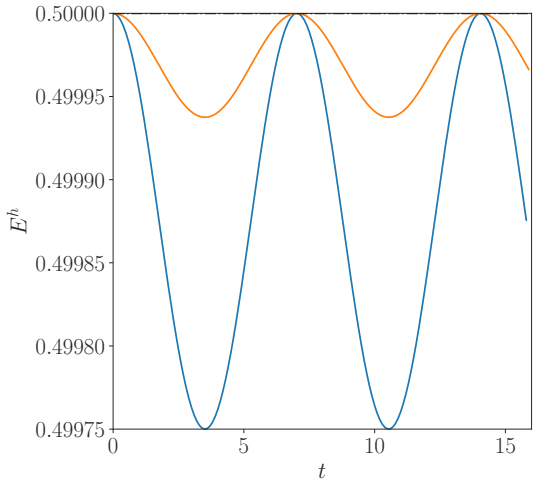

(c) Energy

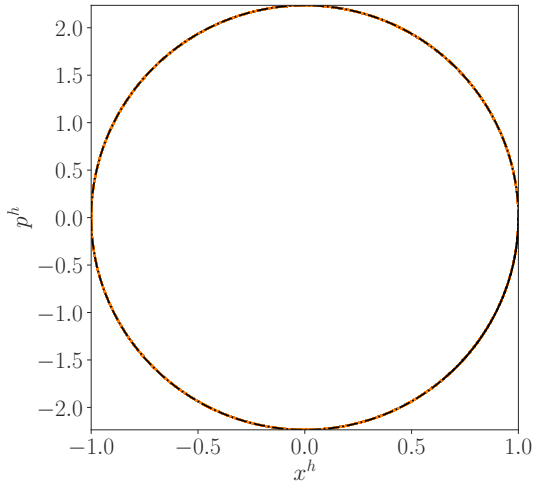

(d) Position - momentum

Figure 4.5: Discrete solution to (4.1) using (4.14) to (4.16). Exact solution shown as $- \cdot -$. Figures 4.4a to 4.4c computed for for $t \in [0, 16]$. Figure 4.4d computed for $t \in [0, 1600]$. $\Delta t = 0.1$ (—), $\Delta t = 0.05$ (—).

4.3 Discretising using the mimetic spectral element method

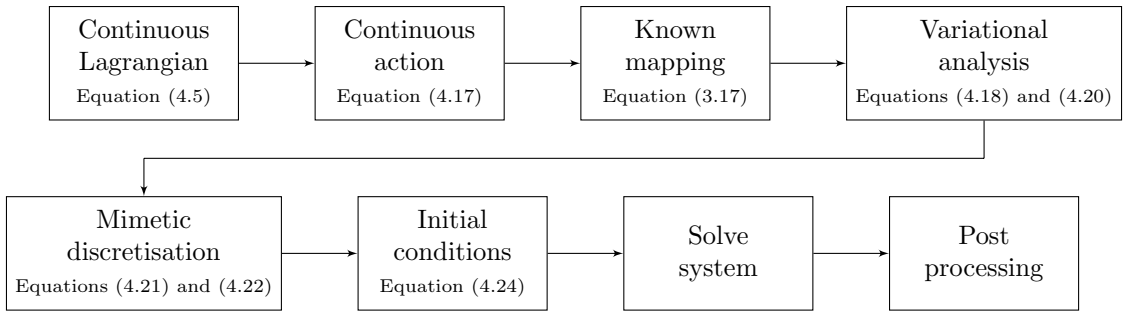

Figure 4.6: Block diagram showing the mimetic spectral element technique with known $\frac{\mathrm{d}t}{\mathrm{d}\tau}(t)$.

In an attempt to improve on the variational integrator technique, this section solves the simple harmonic oscillator problem using the mimetic spectral element technique. A flow diagram is found in Figure 4.6. Let the Lagrangian still be defined as (4.5). Unlike finding the discrete action, a continuous action is sought at first, through

$$\begin{aligned} S(p,x) &= \int_a^b \left[L(x(t),\dot{x}(t),t)\right]\,dt + \int_a^b \left[\dot{p}(t)x(t)\right]\,dt \\ &= \int_a^b \left[\frac{p^2(t)}{2m} - \frac{kx^2(t)}{2}\right]\,dt + \int_a^b \left[\dot{p}(t)x(t)\right]\,dt \end{aligned} \tag{4.17}$$

where the definition of momentum, $p(t) = m\dot{x}(t)$, has been used to replace $\dot{x}(t)$. This means that an additional combination of $p(t)$ and $\dot{x}(t)$ is necessary in order to close the system. The latter will be made clear later in this section. Variational analysis with respect to $p(t)$ results in the definition equation between momentum and velocity through

$$\begin{aligned} \left.\frac{\partial S(x(t),p(t)+\alpha\delta p(t))}{\partial\alpha}\right|_{\alpha=0} &= \int_a^b \left[\frac{p(t)\delta p(t)}{m}\right]\,dt + \int_a^b \left[x(t)\delta\dot{p}(t)\right]\,dt, \\ &= \int_a^b \left[\frac{p(t)}{m}\delta p(t)\right]\,dt - \int_a^b \left[\dot{x}(t)\delta p(t)\right]\,dt + \left[x(t)\delta p(t)\right]_a^b, \\ &= \int_{-1}^1 \left[\frac{p(\tau)}{m}\delta p(\tau)\frac{b-a}{2}\right]\,d\tau - \int_{-1}^1 \left[\dot{x}(\tau)\delta p(\tau)\right]\,d\tau \\ &\quad + \left[x(\tau)\delta p(\tau)\right]_{-1}^1 \quad \forall\delta p(\tau), \end{aligned} \tag{4.18}$$

in which integration by parts is used to convert $\delta\dot{p}(t)$ into $\delta p(t)$. Moreover, $\frac{\mathrm{d}t}{\mathrm{d}\tau} = \frac{b-a}{2}$. Variational analysis with respect to $x(t)$ results in the equation of motion through

$$\left.\frac{\partial S(x(t)+\beta\delta x(t),p(t))}{\partial\beta}\right|_{\beta=0} = \int_a^b \left[-kx(t)\delta x(t)\right]\,dt + \int_a^b \left[\dot{p}(t)\delta x(t)\right]\,dt, \tag{4.19}$$

$$= \int_{-1}^{1}\left[-kx(\tau)\delta x(\tau)\frac{b-a}{2}\right]\,d\tau + \int_{-1}^{1}\left[\dot{p}(\tau)\delta x(\tau)\right]\,d\tau \quad \forall\delta x(\tau). \tag{4.20}$$

The equations of motion follow from (4.18) and (4.20) when again the end points are fixed. This means that again no end point variations are allowed. Furthermore, requiring that (4.18) and (4.20) equal zero for all variations $\delta p(\tau)$ and $\delta x(\tau)$ results in

$$p(\tau)\frac{b-a}{2} = m\dot{x}(\tau) \quad \text{and}$$
$$\dot{p}(\tau) - kx(\tau)\frac{b-a}{2} = 0.$$

Equations (4.18) and (4.20) are discretised using the spectral element technique, in which the variables are related to nodes and edges in one-dimensional space. For this problem, $x(\tau)$ is discretised in nodes on the primal basis denoted as $\bar{x}^h(\tau)$ and $p(\tau)$ is related to nodal dual representation, denoted as $\tilde{p}^h(\tau)$. Equations (4.21) and (4.22) show the discretised variables and are illustrated in Figure 4.7.

$$\begin{aligned}
\bar{x}^h &= \sum_{i=0}^{p} x_i h_i(\tau) \\
\delta\bar{x}^h &= \sum_{i=0}^{p} \delta x_i h_i(\tau) \\
\dot{\bar{x}}^h &= \sum_{i=1}^{p} (x_i - x_{i-1})\, e_i(\tau)
\end{aligned} \tag{4.21}$$

$$\begin{aligned}
\tilde{p}^h &= \sum_{i=1}^{p} p_i e_i'(\tau), \\
\delta\tilde{p}^h &= \sum_{i=1}^{p} \delta p_i e_i'(\tau) \quad \text{and} \\
\dot{\tilde{p}}^h &= \sum_{i=0}^{p} (p_i - p_{i-1})\, h_i'(\tau),
\end{aligned} \tag{4.22}$$

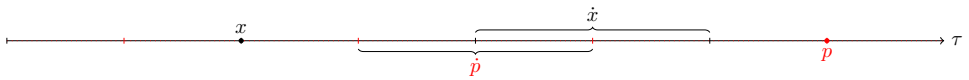

Figure 4.7: Discretised variables from (4.21) and (4.22) displayed on the τ-axis.

Applying (4.21) and (4.22) to (4.18) and (4.20) results in a coupled system between position and momentum. In matrix notation this can be written as

$$\begin{bmatrix} \mathbb{M}_m^{-1} & -\bar{\mathbb{E}}^{(1,0)} \\ \bar{\mathbb{E}}^{(1,0)^T} & -\mathbb{M}_k \end{bmatrix} \begin{bmatrix} \vec{p} \\ \vec{x} \end{bmatrix} = \begin{bmatrix} \vec{0} \\ \vec{0} \end{bmatrix}. \tag{4.23}$$

$\mathbb{M}_m$ and $\mathbb{M}_k$ in (4.23) are shorthand notations for

$$\mathbb{M}_m = \int_{-1}^{1} \left[m e_i(\tau) e_j(\tau) \frac{2}{b-a} \right] d\tau \quad \text{and}$$
$$\mathbb{M}_k = \int_{-1}^{1} \left[k h_i(\tau) h_j(\tau) \frac{b-a}{2} \right] d\tau.$$

The vector to be solved for includes $\vec{p}$ and $\vec{x}$, which read

$$\vec{p} = \begin{bmatrix} p_1 \\ \vdots \\ p_p \end{bmatrix} \quad \text{and} \quad \vec{x} = \begin{bmatrix} x_0 \\ \vdots \\ x_p \end{bmatrix}.$$

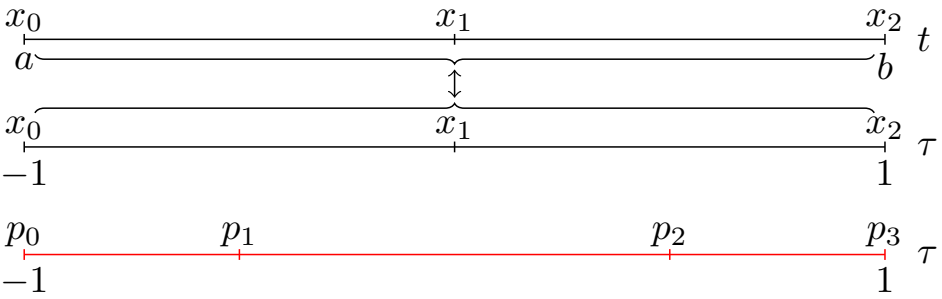

Figure 4.8: Discretised primal and dual space for $a \leq t \leq b$. Figure examplifies mismatch between equations and unknowns. Linear mapping used through (3.16).

Without loss of generality, Figure 4.8 shows the discretised primal and dual space for $a \leq t \leq b$. Here, $x(t)$ is discretised using three primal nodes and $p(t)$ is discretised onto two dual nodes plus two dual nodes on the boundary to be able to calculate $\dot{p}(t)$, adding up to seven unknown values. As a consequence, two extra equations are needed to close the system. To be more specific, the matrix in (4.23) has size 5×7 which cannot be inverted to solve for $\vec{p}$ and $\vec{x}$. The additional two equations are added by means of initial conditions $\hat{x}_0$ and $\hat{p}_0$. The resulting system is

$$\begin{bmatrix} \mathbb{M}_m^{-1} & -\mathbb{E}^{(1,0)} & 0 \\ \mathbb{E}^{(1,0)^T} & -\mathbb{M}_k & \mathbb{N}_x^T \\ 0 & \mathbb{X}^{00} & \mathbb{P}^{10} \end{bmatrix} \begin{bmatrix} \vec{p} \\ \vec{x} \\ \vec{\lambda} \end{bmatrix} = \begin{bmatrix} \vec{0} \\ \vec{0} \\ \vec{\Lambda}_0 \end{bmatrix}, \tag{4.24}$$

with

$$\vec{p} = \begin{bmatrix} p_1 \\ p_2 \end{bmatrix} \quad \text{and} \quad \vec{x} = \begin{bmatrix} x_0 \\ x_1 \\ x_2 \end{bmatrix} \quad \text{and} \quad \vec{\lambda} = \begin{bmatrix} p_0 \\ p_3 \end{bmatrix}$$

$\mathbb{N}_x$ takes size 2×3. Single-entry-matrices $\mathbb{P}^{10}$ and $\mathbb{X}^{00}$ take sizes 2×2 and 2×3 respectively. Their non-zero entry equals one. $\mathbb{P}^{10}$ and $\mathbb{X}^{00}$ read

$$\mathbb{P}^{10} = \begin{bmatrix} 0 & 0 \\ 1 & 0 \end{bmatrix} \quad \text{and} \quad \mathbb{X}^{00} = \begin{bmatrix} 1 & 0 & 0 \\ 0 & 0 & 0 \end{bmatrix}.$$

$\vec{\Lambda}_0$ contains the initial conditions of both $\vec{p}$ and $\vec{x}$ and $\mathbb{N}_x$ relates $\vec{x}$ to its boundary contributors. $\vec{\Lambda}_0$ and $\mathbb{N}_x$ read

$$\vec{\Lambda}_0 = \begin{bmatrix} \hat{x}_0 \\ \hat{p}_0 \end{bmatrix} \quad \text{and} \quad \mathbb{N}_x = \begin{bmatrix} 1 & 0 & 0 \\ 0 & 0 & -1 \end{bmatrix}.$$

The reconstructed polynomials $\tilde{p}^h(t)$, $\bar{x}^h(t)$ and $E^h(t)$ are plotted in Figure 4.9 using (4.21) and (4.22). The average time increment is $\Delta t = \frac{b-a}{p} = 0.1$. Recall (3.13) from Chapter 3, i.e. the energy conservation equation. Its spectral discrete equivalent is represented by

$$\frac{\mathrm{d}}{\mathrm{d}t}\left(\frac{\tilde{p}_i^{h^2}(t)}{2m} + \frac{k\bar{x}_i^{h^2}(t)}{2}\right) = 0 \quad \text{or}$$
$$\frac{\tilde{p}_i^{h^2}(t)}{2m} + \frac{k\bar{x}_i^{h^2}(t)}{2} = E(0),$$

and is shown in Figure 4.9c. It can be seen that discrete energy oscillates but stays between bounds. This is seen in Figure 4.9c. In comparison to Figure 4.4c progression is made, yet no exact energy conservation is found. Looking at Figure 4.9d it is found that for $t \in [0, 1600]$ no inward or outward spiralling is found, meaning that no damping or amplification of the energy level is observed.

Moreover, the definition equation $p(t) = m\dot{x}(t)$ and the constitution equation $\dot{p}(t)+kx(t) = 0$ are shown in Figure 4.10. For $p = 3$ and a timeline split into two segments, the exact and discrete solution are plotted. Figure 4.10a displays both the left-hand-side and the right-hand-side of the definition equation, including its difference in green. The difference is also plotted in Figure 4.10b. It shown that its difference is up to machine precision.

Like Figures 4.10a and 4.10b, Figures 4.10c and 4.10d show the relation between $p(t)$ and $kx(t)$. Again, it is observed that their difference is up to machine precision. From this, it can be concluded that the dual representation of the primal grid can be used to create additional degrees of freedom and that their relation is up to machine precision.

Lastly, p-convergence and Δt-convergence is performed for the system described above. This p- and Δt-convergence is computed for $t \in [0, 16]$ for multiple polynomial degrees and a variety of Δt increments. The error between the exact values and approximated values is computed using the Euclidean norm. It is defined as

$$\left\| \square_{\text{exact}} - \square^h \right\|_2 = \sqrt{\int_a^b \left[\left(\square_{\text{exact}} - \square^h \right)^2 \right]}, \tag{4.25}$$

in which $\square$ equals the quantity of interest. The p-convergence regarding the variables $x(t)$, $p(t)$ and $E(t)$ is found in Figures 4.11a, 4.11c and 4.11e respectively. Δt-convergence regarding the variables $x(t)$, $p(t)$ and $E(t)$ is found in Figures 4.11b, 4.11d and 4.11f.

In Section 4.4 yet another approach is taken in order to conserve energy. This is because it is attempted to conserve the symmetry of the matrix as this is lost by imposing an initial condition on momentum. By allowing an arbitrary mapping between t and τ it is thought to overcome this issue, which will be explained in Section 4.4.

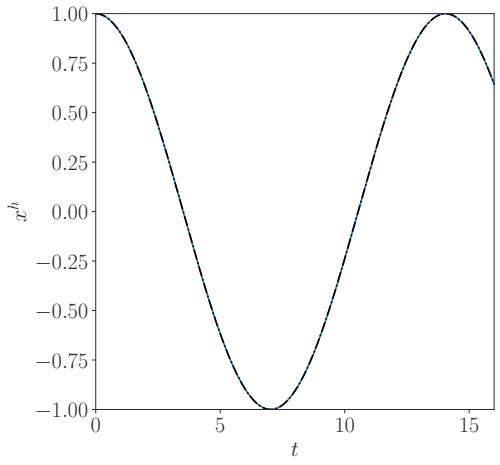

(a) Position

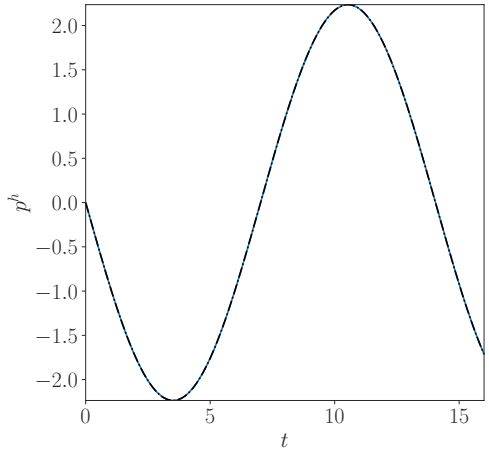

(b) Momentum

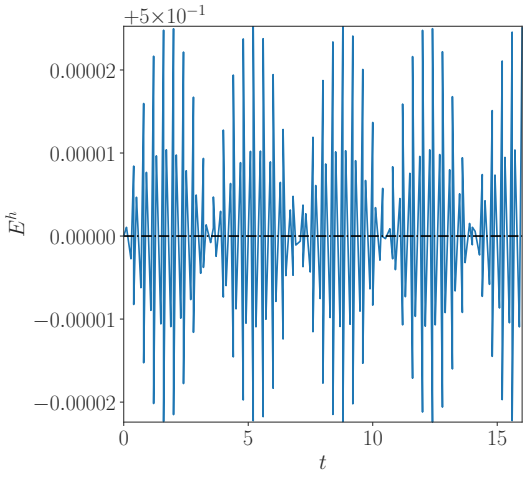

(c) Energy

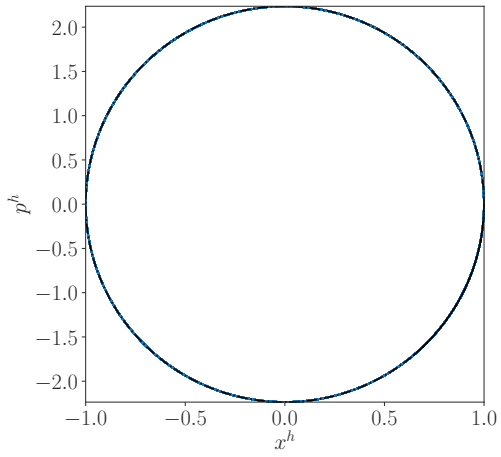

(d) Position - momentum

Figure 4.9: Discrete solution to (4.1) using (4.21), (4.22) and (4.24) using $p = 3$. Exact solution shown as $- \cdot -$. Figures 4.9a to 4.9c computed for $t \in [0, 16]$. Figure 4.9d computed for $t \in [0, 1600]$. $\Delta t = 0.1$ (—).

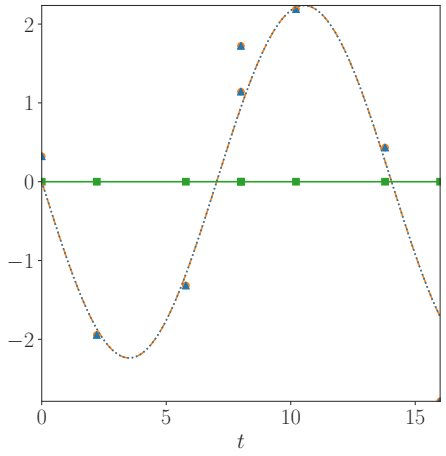

(a) $p^h(t)$ ♦ and $m\dot{x}^h(t)$ ▲ elements from $p^h(t) = m\dot{x}^h(t)$. Difference ■ enlarged in Figure 4.10b.

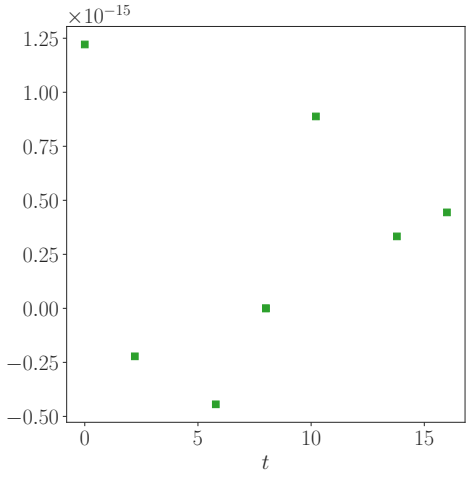

(b) Difference of elements $p^h(t)$ and $m\dot{x}^h(t)$ ■.

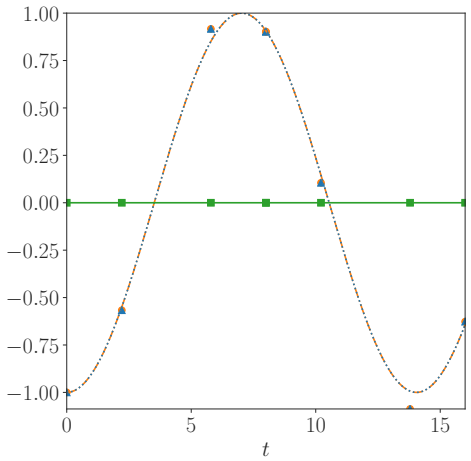

(c) $\dot{p}^h(t)$ ♦ and $-kx^h(t)$ ▲ elements from $\dot{p}^h(t) + kx^h(t) = 0$. Difference enlarged in Figure 4.10d.

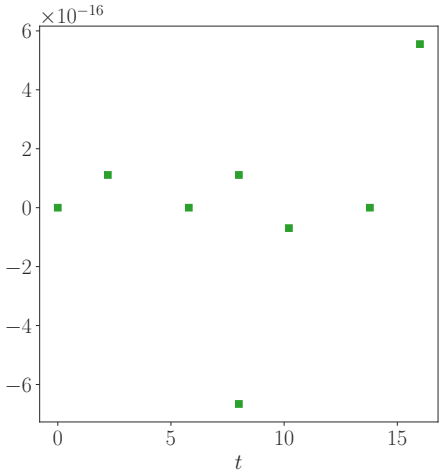

(d) Difference of elements $-kx^h(t)$ and $\dot{p}^h(t)$ ■.

Figure 4.10: Equations of motion $p(t) = m\dot{x}(t)$ and $\dot{p}(t) + kx(t) = 0$ and differences between the left-hand side and right-hand side. Exact solutions $p(t)$ and $\dot{p}(t)$ shown by – · –. Exact solutions $x(t)$ and $\dot{x}(t)$ shown by · · ·. Discrete $p^h(t)$ and $\dot{p}^h(t)$ represented by ♦. Discrete $x^h(t)$ and $\dot{x}^h(t)$ represented by ▲. Exact differences plotted using —. Discrete differences plotted using ■. $\Delta t = 2.29$ using $p = 3$ and $n_e = 2$.

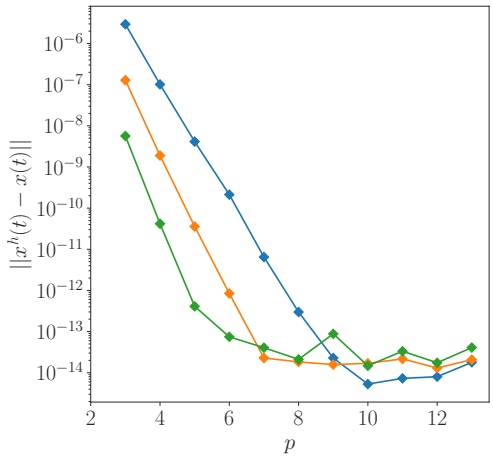

(a) p-convergence for $\vec{x}$ at $\Delta t = 0.1$ (♦), $\Delta t = 0.1$ (♦) and $\Delta t = 0.05$ (♦).

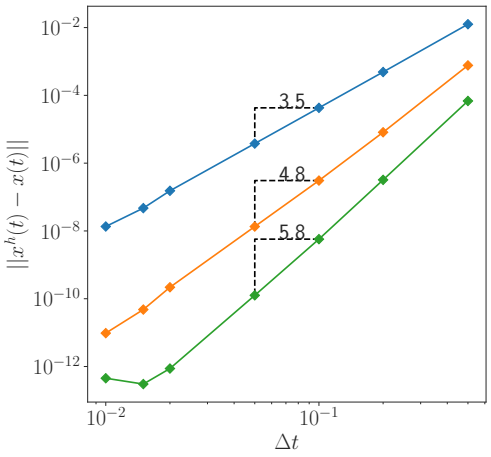

(b) h-convergence for $\vec{x}$ at $p = 2$ (♦), $p = 3$ (♦) and $p = 4$ (♦).

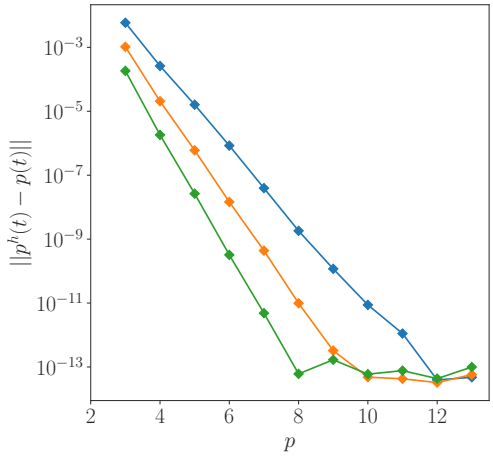

(c) p-convergence for $\vec{p}$ at $\Delta t = 0.2$ (♦), $\Delta t = 0.1$ (♦) and $\Delta t = 0.05$ (♦).

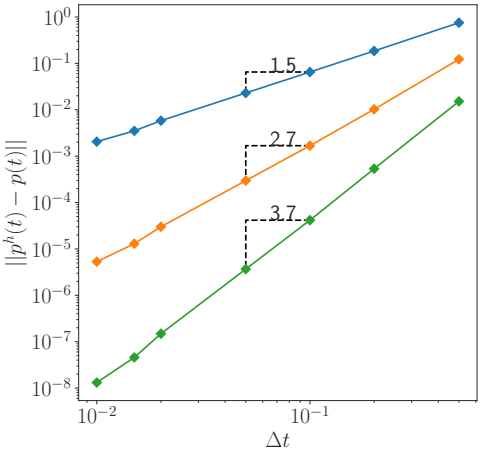

(d) h-convergence for $\vec{p}$ at $p = 2$ (♦), $p = 3$ (♦) and $p = 4$ (♦).

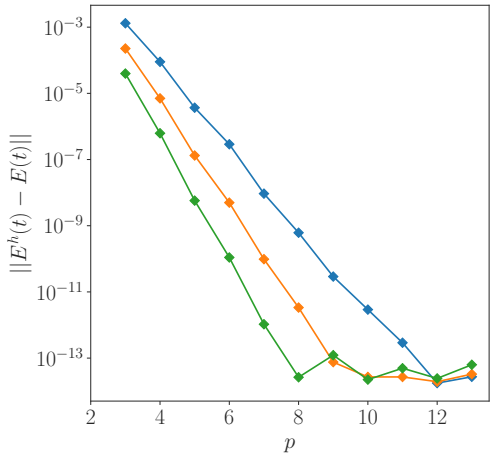

(e) p-convergence for $\vec{E}$ at $\Delta t = 0.2$ (♦), $\Delta t = 0.1$ (♦) and $\Delta t = 0.05$ (♦).

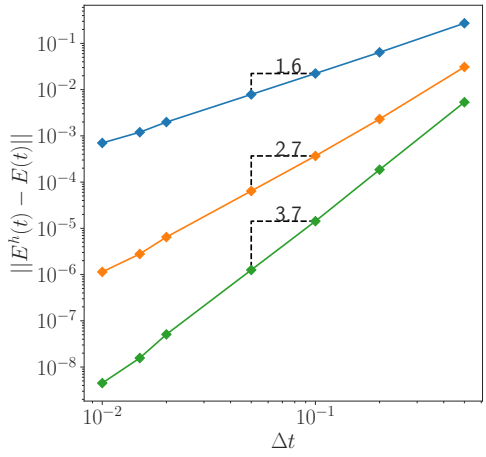

(f) h-convergence for $\vec{E}$ at $p = 2$ (♦), $p = 3$ (♦) and $p = 4$ (♦).

Figure 4.11: p- and Δt-convergence for $p^h(t)$, $x^h(t)$ and $E^h(t)$ of the simple harmonic oscillator problem using (4.21), (4.22) and (4.24). Time interval used: $t \in [0, 16]$.

4.4 Arbitrary linear $t - \tau$ mapping

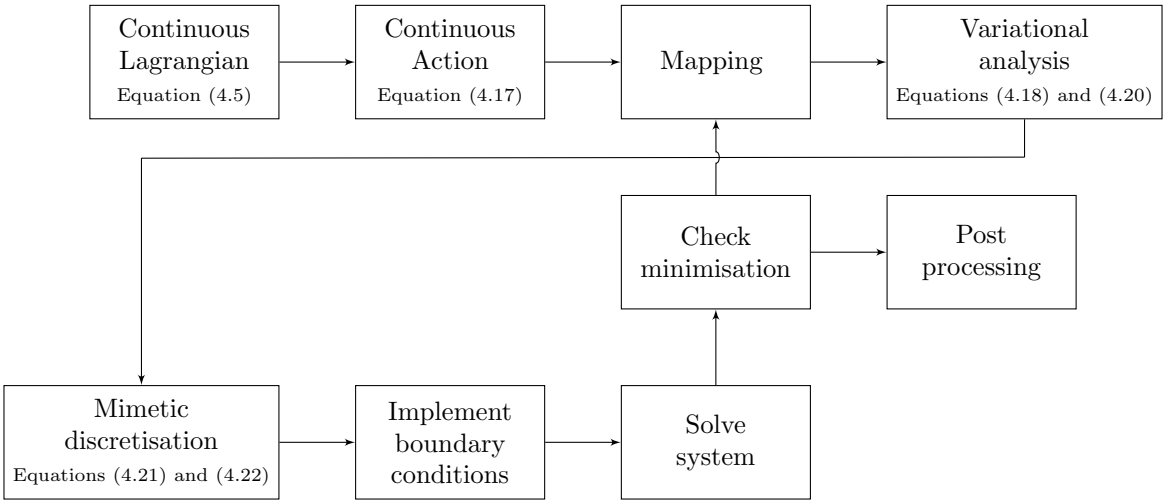

Figure 4.12: Block diagram showing the mimetic spectral element technique with unknown $\frac{\mathrm{d}t}{\mathrm{d}\tau}(\tau)$.

In Section 4.3 a solution to the simple harmonic oscillator was found through a combination of the mimetic spectral element method and a linear transformation between t and τ, through (3.16), based on polynomial degree p and Δt. Improved energy conservation was found in comparison to Section 4.2, yet no exact energy conservation was found when a low polynomial order was used. This section elaborates upon the possibility of adding an unknown to the system in the form of $\frac{\mathrm{d}t}{\mathrm{d}\tau}(\tau)$. An interesting phenomenon occurs when this procedure is followed, of which the flow diagram is found in Figure 4.12. As the a-priori unknown variable $\frac{\mathrm{d}t}{\mathrm{d}\tau}(\tau)$ is incorporated in matrices $\mathbb{M}_m$ and $\mathbb{M}_k$, the solution is found through an iterative process. In the paragraph below Figure 4.12 is explained.

Recall Figure 4.8. Let the initial conditions $x(a)$ and $\dot{x}(a)$ at $t = a$ be known. Through the mapping from t to τ the problem is mapped onto the reference domain $\tau \in [-1, 1]$, introducing $\frac{\mathrm{d}t}{\mathrm{d}\tau}(\tau)$. A position value is *guessed* at the end of the domain in order to have a well-posed problem. Do note that time t at which this position is reached is unknown as the mapping is unknown. As the trajectory of the simple harmonic oscillator can be calculated exactly, x_2 is *guessed* through

$$x_2 = \hat{x}_0 + \hat{\dot{x}}_0 \Delta t + \frac{\hat{\ddot{x}}_0}{2} \Delta t^2, \tag{4.26}$$

in which $\hat{\square}$ represents a known value.The system is then solved using an initial $\frac{\mathrm{d}t}{\mathrm{d}\tau}(\tau)$. After reconstruction, the value of $\tilde{p}^h(t)$ at $t = a$ is compared to the value of $m\hat{\dot{x}}_0$. When

$$\tilde{p}^h \Big|_{\tau=-1} - m\hat{\dot{x}}_0 = 0 \tag{4.27}$$

reaches machine precision, the value for $\frac{\mathrm{d}t}{\mathrm{d}\tau}(\tau)$ at that moment is used to calculate b in $t = b$. The method used to reach machine precision in (4.27) is the Nelder-Mead minimisation method. In short, the Nelder-Mead method uses a $(p+1)$-dimensional simplex on a p-dimensional domain [35]. For the one-dimensional harmonic oscillator problem the simplex is a line, containing two endpoints a and b. The objective is evaluated at both endpoints and sorted. The worst result

is reflected through centroid of all other points, presumably moving the simplex to a minimum. As time is irreversible, $\frac{\mathrm{d}t}{\mathrm{d}\tau}(\tau)$ is restricted to only positive values through

$$\frac{\mathrm{d}t}{\mathrm{d}\tau}(\tau) \geq 0. \tag{4.28}$$

For a more thorough explanation of the Nelder-Mead method, please see [35]. Following the explanation of this arbitrary linear $t-\tau$ mapping, the mathematical derivation is given below. Let the action of the Lagrangian be formulated as

$$\begin{aligned} S(x(t),\dot{x}(t),p(t)) &= \int_a^b \left[T(\dot{x}(t)) - V(x(t))\right]\, dt, + \left[x(t)-\hat{x}\right]p(t)\Big|_{t=a} \\ &\quad + \left[x(t)-\hat{x}\right]p(t)\Big|_{t=b}, \\ &= \int_a^b \left[\frac{1}{2}m\dot{x}^2(t) - \frac{1}{2}kx^2(t)\right]\, dt + \left[x(t)-\hat{x}\right]p(t)\Big|_{t=a} \\ &\quad + \left[x(t)-\hat{x}\right]p(t)\Big|_{t=b}, \end{aligned} \tag{4.29}$$

leading to restrictions formatted through $x(t=a)=\hat{x}|_{t=a}$ and $x(t=b)=\hat{x}|_{t=b}$ by means of Lagrange multipliers $p(t)|_{t=a}$ and $p(t)|_{t=b}$. Mapping to the reference domain by means of *yet* an arbitrary mapping results in

$$\begin{aligned} S(x(\tau),\dot{x}(\tau),p(\tau)) &= \int_{-1}^{1} \left[T(\dot{x}(\tau))\frac{\mathrm{d}\tau}{\mathrm{d}t} - V(x(\tau))\frac{\mathrm{d}t}{\mathrm{d}\tau}\right]\, d\tau, + \left[x(\tau)-\hat{x}\right]p(\tau)\Big|_{\tau=-1} \\ &\quad + \left[x(\tau)-\hat{x}\right]p(\tau)\Big|_{\tau=1}, \\ &= \int_{-1}^{1} \left[\frac{1}{2}m\dot{x}^2(\tau)\frac{\mathrm{d}\tau}{\mathrm{d}t} - \frac{1}{2}kx^2(\tau)\frac{\mathrm{d}t}{\mathrm{d}\tau}\right]\, d\tau + \left[x(\tau)-\hat{x}\right]p(\tau)\Big|_{\tau=-1} \\ &\quad + \left[x(\tau)-\hat{x}\right]p(\tau)\Big|_{\tau=1}. \end{aligned} \tag{4.30}$$

The mapping is arbitrary because $\frac{\mathrm{d}t}{\mathrm{d}\tau}(\tau)$ in (4.30) is unknown, as well as the end-time b in (4.29). Through the minimisation procedure that matches the discrete initial momentum to the exact momentum at t^n, $\frac{\mathrm{d}t}{\mathrm{d}\tau}(\tau)$ and hence b are found. Variational analysis with respect to $x(\tau)$, $p(\tau)|_{\tau=-1}$ and $p(\tau)|_{\tau=1}$ leads to a system of three equations through

$$\left.\frac{\partial S(x(\tau)+\alpha\delta x(\tau),p_{-1},p_1)}{\partial\alpha}\right|_{\alpha=0} = \int_{-1}^{1}\left[m\dot{x}(\tau)\delta\dot{x}(\tau)\frac{\mathrm{d}\tau}{\mathrm{d}t} - kx(\tau)\delta x(\tau)\frac{\mathrm{d}t}{\mathrm{d}\tau}\right]d\tau + \delta x(\tau)p(\tau)\Big|_{\tau=-1} + \delta x(\tau)p(\tau)\Big|_{\tau=1}, \tag{4.31}$$

$$\left.\frac{\partial S(x(\tau),p(\tau)+\beta\delta p(\tau)|_{\tau=-1},p(\tau)|_{\tau=1})}{\partial\beta}\right|_{\beta=0} = [x(\tau)-\hat{x}]\,\delta p(\tau)\Big|_{\tau=-1} \quad \text{and} \tag{4.32}$$

$$\left.\frac{\partial S(x(\tau),p(\tau)|_{\tau=-1},p(\tau)+\gamma\delta p(\tau)|_{\tau=1})}{\partial\gamma}\right|_{\gamma=0} = [x(\tau)-\hat{x}]\,\delta p(\tau)\Big|_{\tau=1}. \tag{4.33}$$

The equations of motion follow from (4.31) to (4.33) when again the end points are fixed, meaning that again the end point variations are not allowed. By equating (4.31) to (4.33) to 0 and using the discretisations mentioned in (4.21) and (4.22) the final system reads

$$\begin{bmatrix}\mathbb{A} & \mathbb{N}^T\\ \mathbb{N} & 0\end{bmatrix}\begin{bmatrix}\vec{x}\\ \vec{\lambda}\end{bmatrix} = \begin{bmatrix}\vec{0}\\ \vec{\Lambda}_0\end{bmatrix}, \tag{4.34}$$

where

$$\mathbb{A} = \bar{\mathbb{E}}^{(1,0)^T}\mathbb{M}_m\bar{\mathbb{E}}^{(1,0)} - \mathbb{M}_k \tag{4.35}$$

and has size $p+1\times p+1$. $\mathbb{M}_m$ and $\mathbb{M}_k$ in (4.35) are shorthand notations for

$$\mathbb{M}_m = \int_{-1}^{1} m\bar{e}_i(\tau)\bar{e}_j(\tau)\frac{\mathrm{d}\tau}{\mathrm{d}t}\,d\tau \quad \text{and}$$
$$\mathbb{M}_k = \int_{-1}^{1} k\bar{h}_i(\tau)\bar{h}_j(\tau)\frac{\mathrm{d}t}{\mathrm{d}\tau}\,d\tau.$$

Furthermore, $\mathbb{N}$ takes size $2\times p+1$ and has non-zero entries at positions $\mathbb{N}^{00}$ and $\mathbb{N}^{1p}$ which have a value of 1. $\vec{\lambda}$ contains the entries p_0 and p_{p+1} and $\vec{\Lambda}_0$ encompasses $\hat{x}_0$ and $\hat{x}_p$. $\mathbb{N}$ and $\vec{\Lambda_0}$ read

$$\mathbb{N} = \begin{bmatrix}1 & 0 & \cdots & 0 & 0\\ 0 & 0 & \cdots & 0 & 1\end{bmatrix} \quad \text{and} \quad \vec{\Lambda}_0 = \begin{bmatrix}\hat{x}_0\\ \hat{x}_p\end{bmatrix}.$$

The vectors $\vec{x}$ and $\vec{\lambda}$ read

$$\vec{x} = \begin{bmatrix}x_0\\ \vdots\\ x_p\end{bmatrix} \quad \text{and} \quad \vec{\lambda} = \begin{bmatrix}p_0\\ p_{p+1}\end{bmatrix}.$$

The fraction $\frac{\mathrm{d}t}{\mathrm{d}\tau}(\tau)$ is found through the minimisation described above and the mapping

$$\begin{aligned} t(\tau) &= a\tau + b,\\ &= \frac{\mathrm{d}t}{\mathrm{d}\tau}\tau + t^n + \frac{\mathrm{d}t}{\mathrm{d}\tau}, \end{aligned} \tag{4.36}$$

is thereafter constructed. The solution is then reconstructed and the procedure is repeated. A test case similar to the test case used in Sections 4.2 and 4.3 is investigated. The results are found in Figure 4.13 for $p = 3$ and $\Delta t \approx 0.1$. It is seen that position and momentum in Figure 4.13a and Figure 4.13b respectively display a close match with respect to the exact solution. It is however clearly visible that the total energy tends to run away from the exact solution. This is shown in Figure 4.13c. The position-momentum plot in Figure 4.13d for $t \in [0, 1600]$ however indicates that the divergence of the energy is small. A reason for the increasing energy may be found in the establishment of x_p. Recalling (4.26), it might be that this guess will be outside the range in which a solution is possible, resulting in a minimisation procedure that will not be properly minimised. It is therefore that a jump is seen at the trough of the position plot.

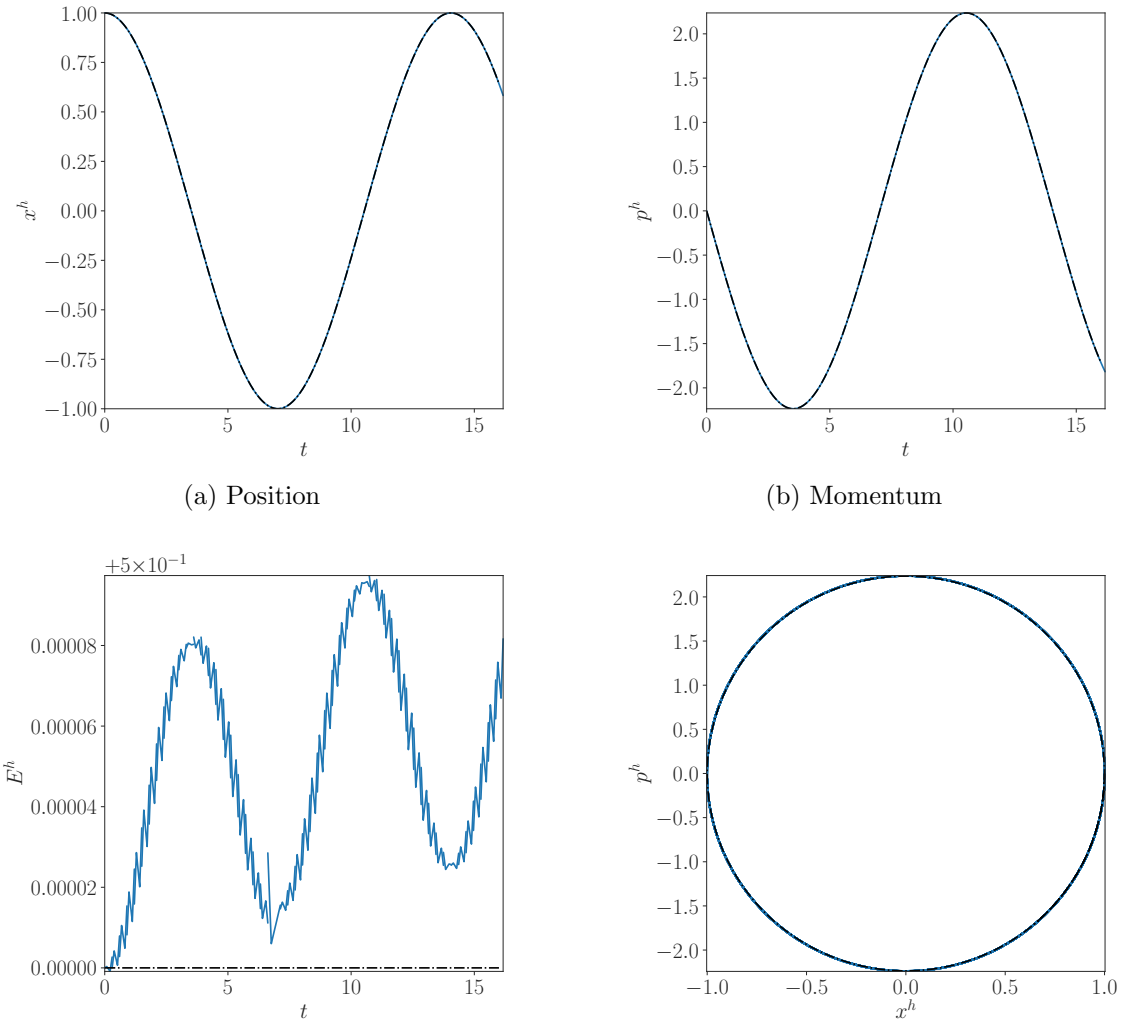

(a) Position

(b) Momentum

(c) Energy

(d) Position - momentum

Figure 4.13: Discrete solution to (4.1) using (4.21), (4.22) and (4.34) using $p = 3$. Exact solution shown as $- \cdot -$. Figures 4.13a to 4.13c computed for for $t \in [0, 16]$. Figure 4.13d computed for $t \in [0, 1600]$. $\Delta t = 0.1$ (—).

4.5 Spectral marching methods

Recall that the main problem faced in this report is the challenge to deal with the future boundary condition when variational analysis is applied. See for example Sections 1.2 and 3.2. In the former sections it was tried to cope with the aforementioned in a variety of ways. The approach in this section incorporates the best of all methods described above.

Let the discretisation method start by recapping the challenges faced in Sections 4.3 and 4.4. In Section 4.3, a primal and a dual grid were used to compute the solution. Furthermore, the matrix in (4.24) was asymmetric. The method also incorporated a known mapping between t and τ and no time marching was incorporated.

The method described in Section 4.4 on the other hand used time marching and included a symmetric matrix in (4.34). The downside of this method was that it relied on the minimisation procedure to find the initial momentum. The method that will be described below includes the marching from Section 4.4 and the asymmetric layout of Section 4.3. Two variations will be discussed, of which the solutions are shown in Figures 4.14 and 4.16 respectively.

Recall (4.34) and (4.35) with

$$\mathbb{M}_m = \int_{-1}^{1} m\bar{e}_i(\tau)\bar{e}_j(\tau)\frac{\mathrm{d}\tau}{\mathrm{d}t}\,d\tau \quad \text{and}$$
$$\mathbb{M}_k = \int_{-1}^{1} k\bar{h}_i(\tau)\bar{h}_j(\tau)\frac{\mathrm{d}t}{\mathrm{d}\tau}\,d\tau.$$

The mapping between t and τ is done as described in Section 3.4 such that

$$\frac{\mathrm{d}t}{\mathrm{d}\tau} = 0.1\frac{p}{2},$$

meaning that the interval between primal nodes equals 0.1. Here, p represents the polynomial degree. The two spectral marching methods described in this section differ in their accompanying matrix $\mathbb{N}$. Focusing on the first method, matrices $\mathbb{N}$ and $\vec{\Lambda}_0$ read

$$\mathbb{N} = \begin{bmatrix} 1 & 0 & \cdots & 0 & 0 \end{bmatrix} \quad \text{and} \quad \vec{\Lambda}_0 = \begin{bmatrix} \hat{x}_0 \end{bmatrix}.$$

The vector $\vec{x}$ and $\vec{\lambda}$ read

$$\vec{x} = \begin{bmatrix} x_0 \\ \vdots \\ x_p \end{bmatrix} \quad \text{and} \quad \vec{\lambda} = \begin{bmatrix} \hat{p}_0 \end{bmatrix}.$$

The system is thereafter rearranged to end with known values at the right-hand side. This

is done through

$$\begin{bmatrix} \mathbb{A} & \mathbb{B}^T \\ \mathbb{N} & 0 \end{bmatrix} \begin{bmatrix} x_0 \\ \vdots \\ x_p \\ \hat{p}_0 \end{bmatrix} = \begin{bmatrix} 0 \\ \vdots \\ 0 \\ \hat{x}_0 \end{bmatrix}, \qquad \begin{bmatrix} \mathbb{A} \\ \mathbb{N} \end{bmatrix} \begin{bmatrix} x_0 \\ \vdots \\ x_p \end{bmatrix} = \begin{bmatrix} -\hat{p}_0 \\ 0 \\ \vdots \\ 0 \\ \hat{x}_0 \end{bmatrix}, \tag{4.37}$$

where $\mathbb{B}$ reads

$$\mathbb{B} = \begin{bmatrix} 1 & 0 & \cdots & 0 \end{bmatrix}.$$

The solution of (4.37) only solves for position though. The momentum p_{p+1} at the end of the domain is calculated through energy conservation. This can be done since energy at $t = 0$ is known to be

$$E_0 = \frac{1}{2m} p_0^2 + \frac{1}{2} k x_0^2, \tag{4.38}$$

resulting in the expression for p_{p+1}

$$p_{p+1} = \sqrt{2mE_0 - kmx_p^2}. \tag{4.39}$$

Equation (4.39) sets the (deviating) energy curve $E(t)$ back to its initial energy level, causing possible jumps. The results of this system can be found in Figure 4.14. Furthermore, p- and Δt-convergence has been computed. This is shown in Figure 4.15.

The other spectral marching method takes the endpoint into consideration. The matrix $\mathbb{N}$ and $\vec{\Lambda}_0$ therefore read

$$\mathbb{N} = \begin{bmatrix} 1 & 0 & \cdots & 0 & 0 \\ 0 & 0 & \cdots & 0 & 1 \end{bmatrix} \quad \text{and} \quad \vec{\Lambda}_0 = \begin{bmatrix} \hat{x}_0 \\ \hat{x}_p \end{bmatrix}.$$

This version of the spectral marching method moves initial position x_0 and initial momentum

p_0 to the right-hand side of the system. This is done through

$$\begin{bmatrix} \mathbb{A} & \mathbb{N}^T \\ \mathbb{N} & 0 \end{bmatrix} \begin{bmatrix} x_0 \\ \vdots \\ x_p \\ \hat{p}_0 \\ p_{p+1} \end{bmatrix} = \begin{bmatrix} 0 \\ \vdots \\ 0 \\ \hat{x}_0 \\ x_p \end{bmatrix},$$

$$\begin{bmatrix} \mathbb{A} & \mathbb{B}^T \\ \mathbb{N} & 0 \end{bmatrix} \begin{bmatrix} x_0 \\ \vdots \\ x_p \\ p_{p+1} \end{bmatrix} - \begin{bmatrix} 0 \\ \vdots \\ 0 \\ x_p \end{bmatrix} = \begin{bmatrix} 0 \\ \vdots \\ 0 \\ \hat{x}_0 \\ 0 \end{bmatrix} - \begin{bmatrix} \hat{p}_0 \\ 0 \\ \vdots \\ 0 \end{bmatrix} \quad \text{and} \tag{4.40}$$

$$\begin{bmatrix} \mathbb{A} & \mathbb{C}^T \\ \mathbb{N} & \mathbb{D} \end{bmatrix} \begin{bmatrix} x_0 \\ \vdots \\ x_p \\ p_{p+1} \\ x_p \end{bmatrix} = \begin{bmatrix} -\hat{p}_0 \\ 0 \\ \vdots \\ 0 \\ \hat{x}_0 \\ 0 \end{bmatrix}.$$

Here, $\mathbb{B}$, $\mathbb{C}$ and $\mathbb{D}$ read

$$\mathbb{B} = \begin{bmatrix} 0 & \cdots & 0 & -1 \end{bmatrix}, \quad \mathbb{C} = \begin{bmatrix} 0 & \cdots & 0 & -1 \\ 0 & \cdots & 0 & 0 \end{bmatrix} \quad \text{and} \quad \mathbb{D} = \begin{bmatrix} 0 & 0 \\ 0 & -1 \end{bmatrix}.$$

Solving the system in (4.40) results in finding p_{p+1} and x_p which can subsequently be used for the next computation. The results are shown in Figure 4.16. Furthermore p-convergence and Δt-convergence is computed and can be found in Figure 4.17.

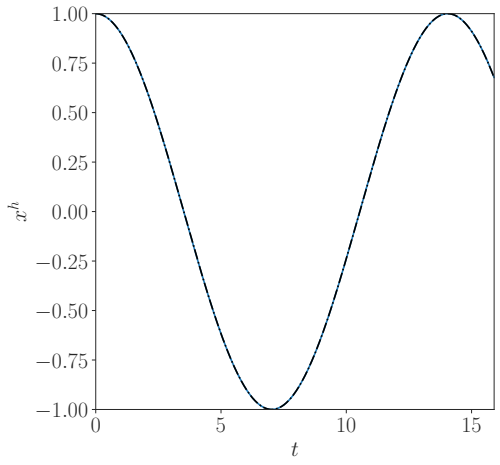

(a) Position

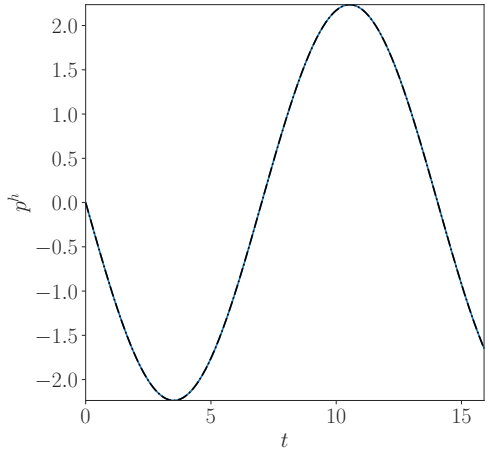

(b) Momentum

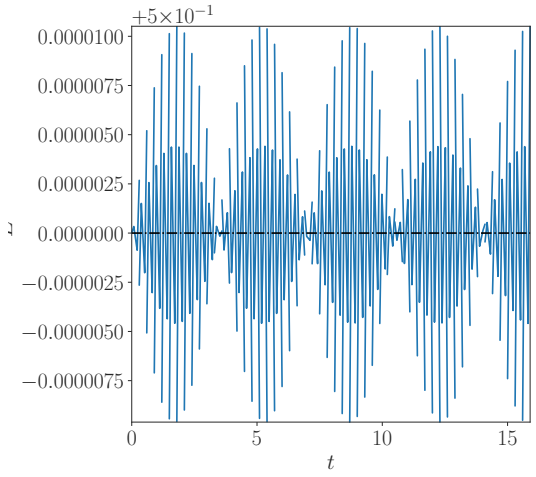

(c) Energy

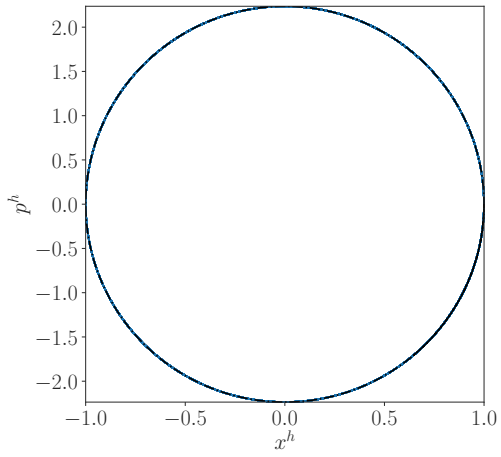

(d) Position - momentum

Figure 4.14: Discrete solution to (4.1) using (4.21), (4.22) and (4.37) using $p = 3$. Exact solution shown as $- \cdot -$. Figures 4.14a to 4.14c computed for for $t \in [0, 16]$. Figure 4.14d computed for $t \in [0, 1600]$. $\Delta t = 0.1$ (—).

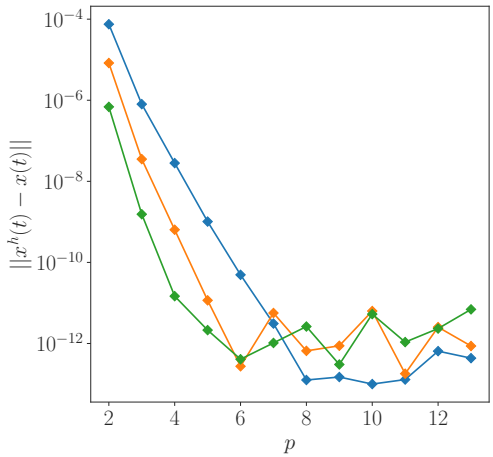

(a) p-convergence for $\vec{x}$ at $\Delta t = 0.2$ (♦), $\Delta t = 0.1$ (♦) and $\Delta t = 0.05$ (♦).

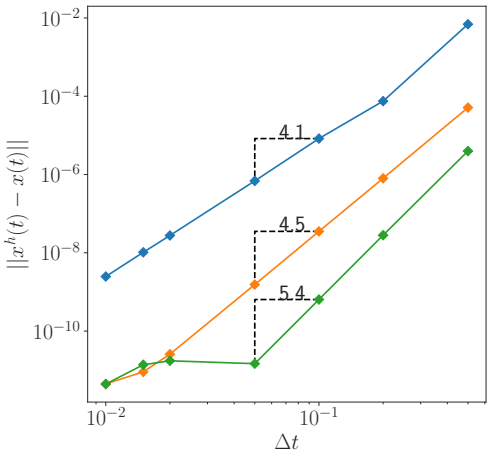

(b) h-convergence for $\vec{x}$ at $p = 2$ (♦), $p = 3$ (♦) and $p = 4$ (♦).

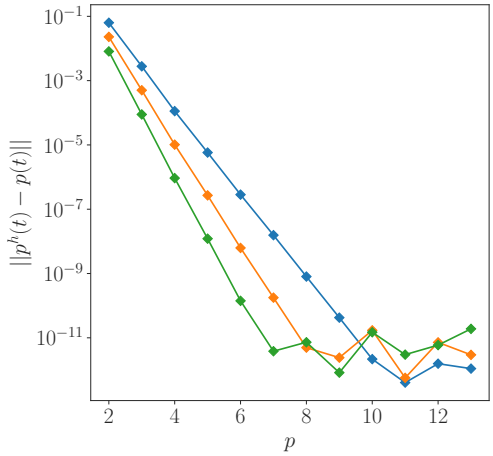

(c) p-convergence for $\vec{p}$ at $\Delta t = 0.2$ (♦), $\Delta t = 0.1$ (♦) and $\Delta t = 0.05$ (♦).

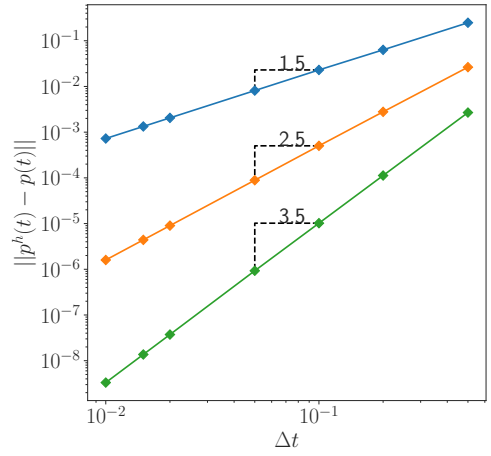

(d) h-convergence for $\vec{p}$ at $p = 2$ (♦), $p = 3$ (♦) and $p = 4$ (♦).

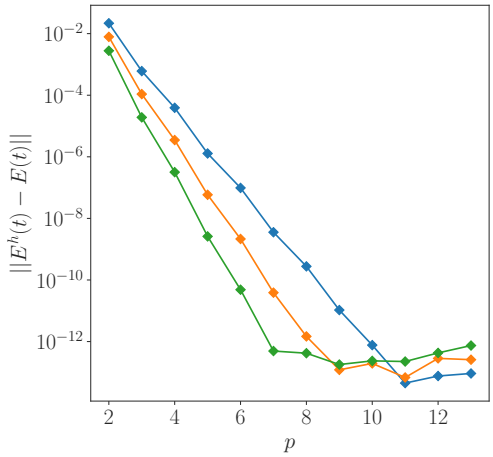

(e) p-convergence for $\vec{E}$ at $\Delta t = 0.2$ (♦), $\Delta t = 0.1$ (♦) and $\Delta t = 0.05$ (♦).

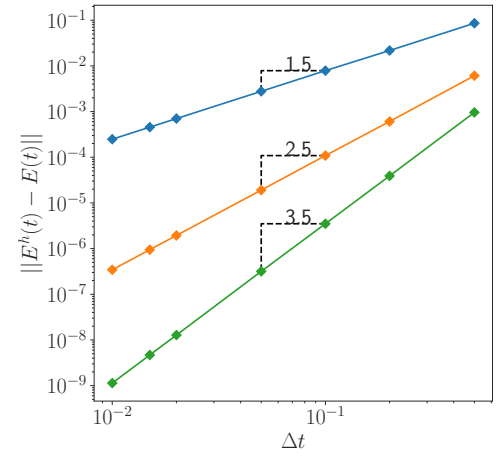

(f) h-convergence for $\vec{E}$ at $p = 2$ (♦), $p = 3$ (♦) and $p = 4$ (♦).

Figure 4.15: p- and Δt-convergence for p, x and E of the simple harmonic oscillator problem using (4.21), (4.22) and (4.37).

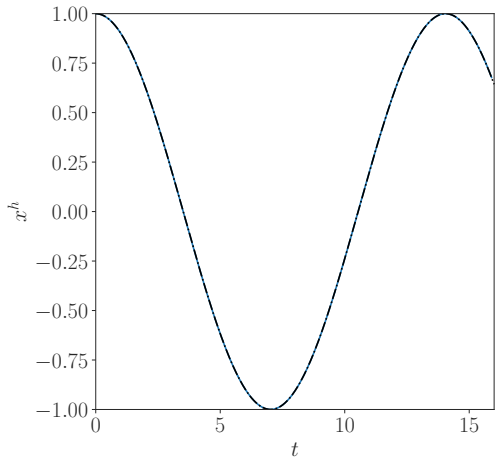

(a) Position

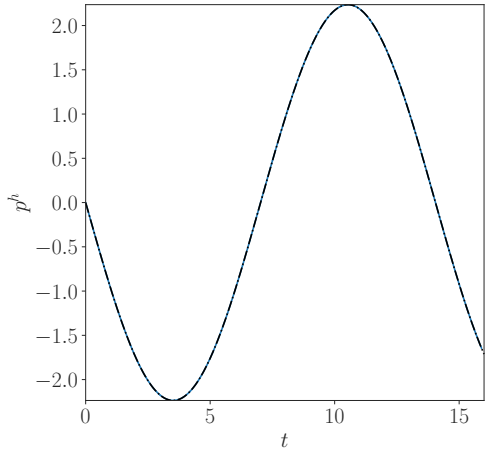

(b) Momentum

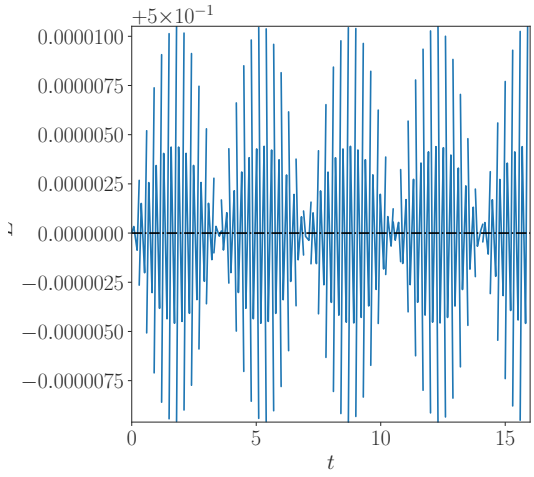

(c) Energy

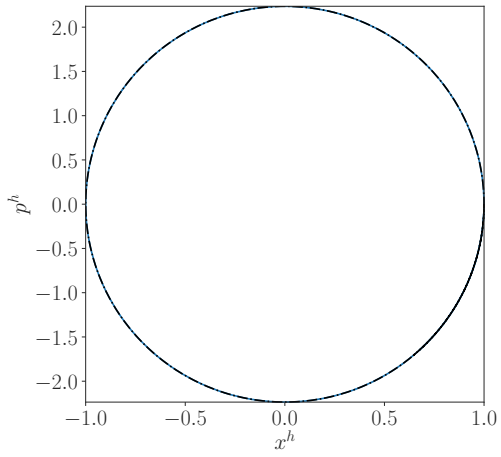

(d) Position - momentum

Figure 4.16: Discrete solution to (4.1) using (4.21), (4.22) and (4.40) using $p = 3$. Exact solution shown as $- \cdot -$. Figures 4.16a to 4.16c computed for for $t \in [0, 16]$. Figure 4.16d computed for $t \in [0, 1600]$. $\Delta t = 0.1$ (—).

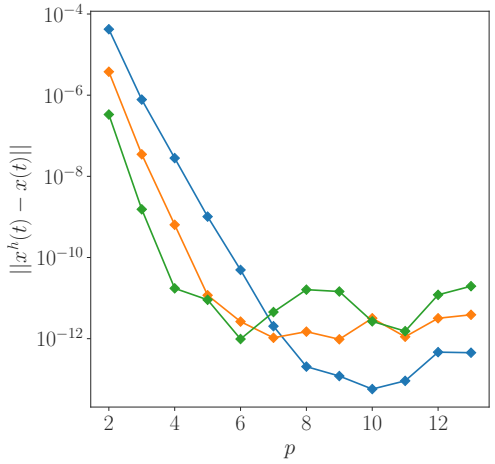

(a) p-convergence for $\vec{x}$ at $\Delta t = 0.2$ (♦), $\Delta t = 0.1$ (♦) and $\Delta t = 0.05$ (♦).

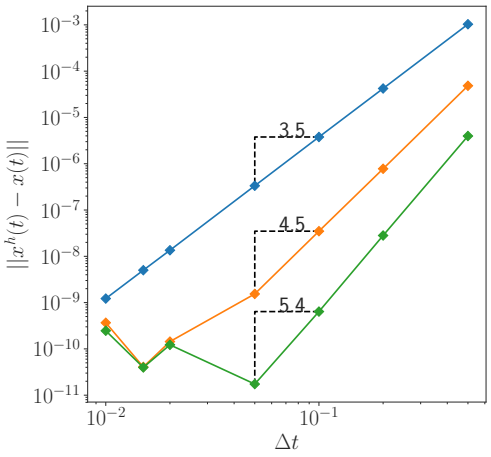

(b) h-convergence for $\vec{x}$ at $p = 2$ (♦), $p = 3$ (♦) and $p = 4$ (♦).

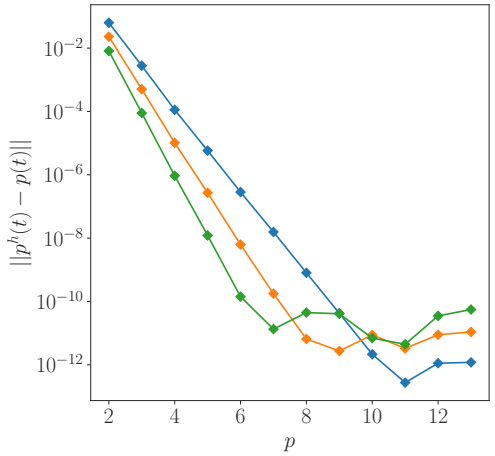

(c) p-convergence for $\vec{p}$ at $\Delta t = 0.2$ (♦), $\Delta t = 0.1$ (♦) and $\Delta t = 0.05$ (♦).

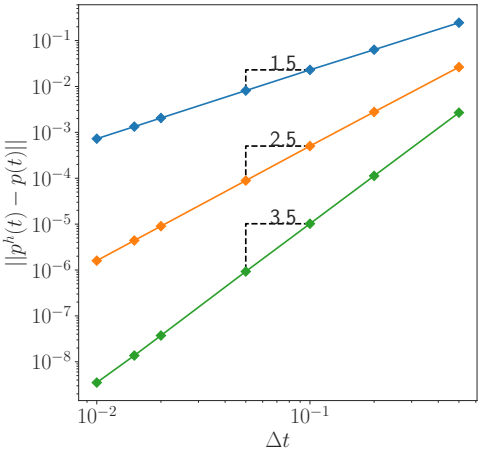

(d) h-convergence for $\vec{p}$ at $p = 2$ (♦), $p = 3$ (♦) and $p = 4$ (♦).

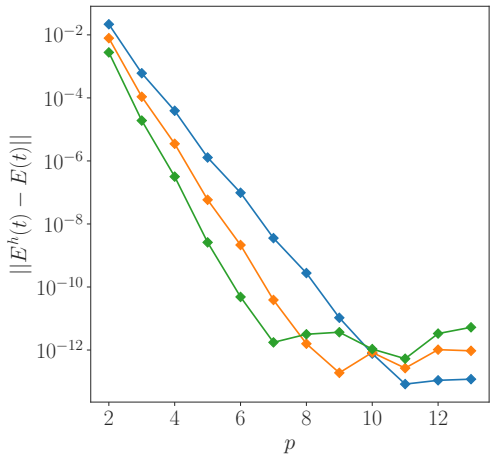

(e) p-convergence for $\vec{E}$ at $\Delta t = 0.2$ (♦), $\Delta t = 0.1$ (♦) and $\Delta t = 0.05$ (♦).

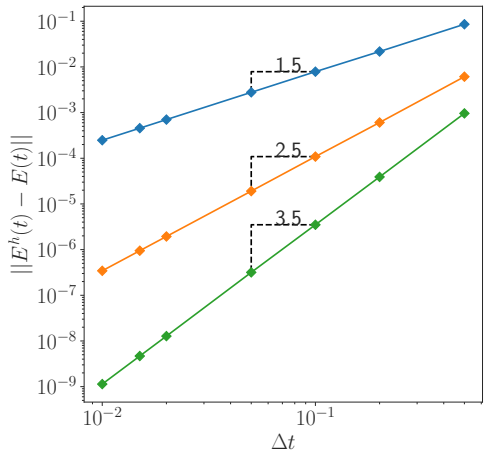

(f) h-convergence for $\vec{E}$ at $p = 2$ (♦), $p = 3$ (♦) and $p = 4$ (♦).

Figure 4.17: p- and Δt-convergence for p, x and E of the simple harmonic oscillator problem using (4.21), (4.22) and (4.40).

4.6 Summary

This chapter covered the discretisation of a simple harmonic oscillator. Through a discrete Lagrangian in Section 4.2 and through mimetic spectral element discretisation in Sections 4.3 to 4.5 discrete solutions were found. Section 4.4 reformulated the mimetic spectral element method and changed the method in a *marching* method by means of an arbitrary linear $t - \tau$ mapping. Section 4.5 combined the best of both derivations in Sections 4.3 and 4.4 to arrive at another formulation. This section takes all methods together and compares them with each other. The focus will be on energy conservation.

The variational integrator technique in Section 4.2 that uses (4.10) has a mismatch when one compares discrete momentum and exact momentum at $t = 0$. This is shown in Figure 4.4b, but is for the sake of clarity enlarged in Figure 4.18a. The corresponding energy behaviour is shown in Figure 4.4c. It can be seen that discrete energy is oscillatory around the exact energy level but bounded and that the maximum deviation between the exact energy level and discrete energy is approximately 10^{-2}.

The variational integrator technique in Section 4.2 that uses (4.12) has no mismatch when comparing exact and discrete momentum at $t = 0$. This is shown once more in Figure 4.18b. The energy level of this technique also oscillates but on the contrary to the aforementioned variational technique, this technique never exceeds the exact energy level. The maximum deviation between the exact energy level and discrete energy level is significantly smaller compared to the aforementioned method and is approximately 2.5×10^{-4}. This is 40 times smaller.

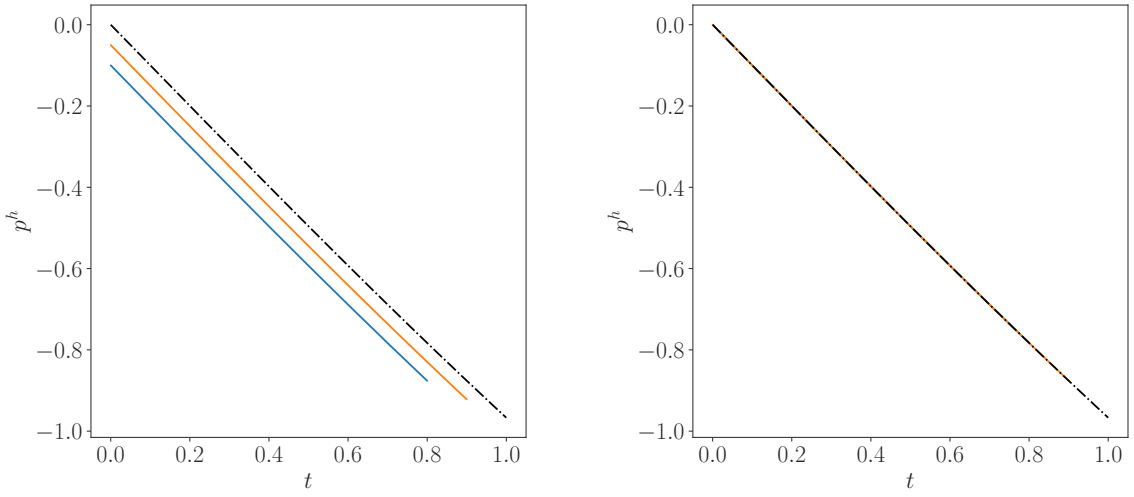

(a) Momentum using (4.10)

(b) Momentum using (4.15)

Figure 4.18: Enlarged cut outs from Figures 4.4b and 4.5b to indicate the mismatch in Figure 4.18a and the matching initial momentum in Figure 4.18b.

Both variational integrator techniques display a decreasing maximum amplitude when the timestep is smaller. For $\Delta t = 0.05$ instead of $\Delta t = 0.1$, the maximum deviations from the exact energy level are approximately 5×10^{-3} and 5×10^{-5} respectively. This means that halving the timestep the maximum deviation decreases 2 and 5 respectively. Based on these findings it can be concluded that the latter variational integrator technique converges faster to the exact energy level in comparison to the former.

Looking at the results found in Section 4.3, it is found that the maximum deviation reads approximately 2×10^{-5} for $p = 3$ and $\Delta t = 0.1$. Again, it is shown that energy oscillates around

the exact energy level and does not amplify nor damp out. The position and momentum also captured the desired physics.

The total opposite happened when a marching method was attempted using a forecasting method and arbitrary $t - \tau$ mapping in Section 4.4. Energy gradually and linearly increased over time, possibly due to curvature problems.

At last, two spectral marching methods were investigated. They captured the most promising aspects from all previously described methods. Both methods have similar performance, having a maximum energy deviation of 1×10^{-5} for $p = 3$ and $\Delta t = 0.1$. The latter spectral marching technique however, did not rely on an energy setback at the end of an interval.

A comparison among all different approaches is shown in Table 4.1. The most promising technique is the last one, because of its robustness and simplicity.

Table 4.1: Comparison maximum energy deviation $E_{\max}$ from $E(t)$.

			$\Delta t = 0.1$	$\Delta t = 0.05$
		p	E_{max} - $E(t)$	E_{max} - $E(t)$
VIT 1	(Figure 4.4)	-	10^{-2}	5×10^{-3}
VIT 2	(Figure 4.5)	-	2.5×10^{-4}	5×10^{-5}
MSEM 1	(Figure 4.9)	3	2×10^{-5}	-
MSEM 2	(Figure 4.13)	3	-	-
SMM 1	(Figure 4.14)	3	1×10^{-5}	1×10^{-6}
SMM 2	(Figure 4.16)	3	1×10^{-5}	1×10^{-6}

5 Conclusion

This thesis focused on developing a discretisation technique that conserved energy up to machine precision by using the mimetic spectral element method. Deriving a mimetic spectral element technique for time-dependent problems turned out to raise some challenges, which will be addressed in the next paragraphs. This chapter reflects on the research questions and research objective in Section 5.1, after which it concludes with recommendations in Section 5.2.

The first challenge that had to be dealt with turned out to be the boundary conditions on either side of the time domain. Derived from a Lagrangian formulation and integrated the latter by parts resulted in explicit boundary contributions on both sides of the time domain. This could be dealt with on a spatial domain as Dirichlet or Neumann boundary conditions could be set on either side of the domain. On the contrary however, boundaries conditions on the time domain can only be specified on the boundary that deals with the present. It was coped with through an arbitrary mapping between the real time domain and a reference domain, see Section 4.4. Through this method it was possible to restrict the real time domain on both boundaries, yet without a time stamp because the mapping was not known. Later in Section 4.5, another workaround was found to cope with the future boundary.

Another challenge that was faced, was found in the translation from continuous time-dependent problems to discrete time-dependent problems using the mimetic spectral element method. A second order time-dependent problem requires 2 initial conditions for it to have a unique solution, i.e. an initial position and initial velocity. Its discrete equivalent, due to the problem that was mentioned in the previous paragraph, had only one initial condition. Through a minimisation procedure the mapping between the real time domain and the reference time domain was chosen such that the Lagrange multiplier took the desired initial condition value.

It was shown that all methods did not succeed in achieving energy conservation up to machine precision, but showed oscillating energy behaviour. The variational integrator techniques were outperformed by the spectral element techniques as the latter had a smaller error. It was furthermore shown that p- and Δt-convergence allowed energy conservation when a higher polynomial order was chosen.

Section 4.4 showed that forecasting position behaviour is not necessarily a good alternative for dealing with future boundaries. The most promising technique was found to be the spectral marching method from Section 4.5, which turned out to be the most simplistic and robust method.

5.1 Reflecting on the research objective and research questions

In Chapter 1 it was stated that this thesis aimed

Research Objective

> to further develop the mimetic spectral element method in its fourth dimension time by critically reflecting on the core concepts of differential topology, algebraic topol-

ogy and mimetic operators of the mimetic spectral element method and Lagrangian and Hamiltonian mechanics.

Based on the findings retrieved and challenges faced when solving the simple harmonic oscillator problem in Chapter 4, it was concluded that progressing the mimetic spectral element method in its fourth dimension time was primarily focused on conserving energy. The Lagrangian and Hamiltonian mechanics in combination with the mimetic operators and algebraic topology ensured energy conservation at a continuous level, yet not on a discretised domain.

Research Questions

1) How does time-dependence fit in the mimetic spectral element method?

2) Why have not yet other engineers tried (or succeeded) to solve time-dependent problems using the mimetic spectral element method?

3) Is it possible to discretise time in a similar way as space is discritsed according to the mimetic spectral element method?

Research Question 3) can be answered straight away. Yes, it time-dependent variables can be discretised in a similar fashion with respect to spatial variables. This also answers Research Question 1) partially. time-dependence can be fit in the mimetic spectral element method rather easily. The problem arises however when variational analysis is applied to the method, creating the boundaries. To fit time-dependence, those boundaries were best treated by considering no end point variations. Reconsidering Research Question 2), it must be said that other people did consider the combination of time-dependence and the mimetic spectral element method, see for example [18]. It has however never been applied using the mimetic spectral element method for time variables.

5.2 Recommendations for future work

This thesis focused on mimicking the physical behaviour of a one-dimensional simple harmonic oscillator, which meant that only a single point in space was solved. Proceeding challenges that are found interesting and contribute to using the mimetic spectral element method for time-dependent problems are listed in the next paragraphs.

A first extension of the simple harmonic oscillator problem would be to solve the same problem with multiple bodies instead. An illustration of this system is found in Figure 5.1a. The behaviour of this system is chaotic and not oscillatory and proves to be highly sensitive to its initial conditions.

Another field of interest is the one-dimensional wave equation. This second order differential equation in both space and time requires special attention of the time boundary dealing with the future. A representation of this motion is shown in Figure 5.1b. A first exploration has already been done. The wave equation can be solved by discretising the accompanied Lagrangian, reading

$$S(p,x,N) = \int_a^b \int_0^T \left[\frac{1}{2}p\dot{x} - \frac{1}{2}\epsilon N\right] dt\,dx + \int_a^b \int_0^T \left[x\left(\frac{\partial p}{\partial t} - \frac{\partial N}{\partial x}\right)\right] dt\,dx + \int_a^b \left[(x-\hat{x})\,\lambda\Big|_0^T\right] dx + \int_0^T \left[(x-\hat{x})\,\lambda\Big|_a^b\right] dt.$$

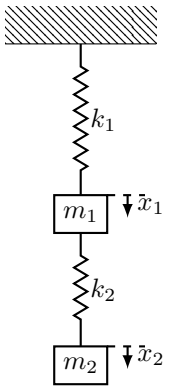

(a) Undamped multiple mass spring system.

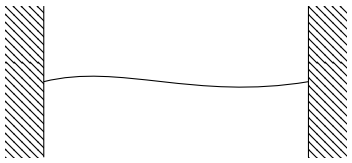

(b) Undamped one-dimensional wave system.

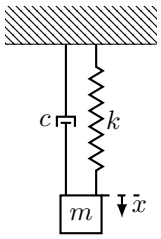

(c) Damped simple harmonic oscillator

Figure 5.1: Recommended systems for future work.

Using the relation between velocity and momentum

$$p = \rho A \dot{x},$$

and the relation between stress and strain

$$N = EA\epsilon,$$

the expression becomes

$$S(p,x,N) = \int_a^b \int_0^T \left[\frac{1}{2}\frac{p^2}{\rho A} - \frac{1}{2}\frac{N^2}{EA}\right] dt\,dx + \int_a^b \int_0^T \left[x\left(\frac{\partial p}{\partial t} - \frac{\partial N}{\partial x}\right)\right] dt\,dx + \int_a^b \left[(x-\hat{x})\,\lambda\Big|_0^T\right] dx + \int_0^T \left[(x-\hat{x})\,\lambda\Big|_a^b\right] dt.$$

Taking care of the boundary conditions in space and doing variational analysis results in the equation of motion and the constitutive equations, reading

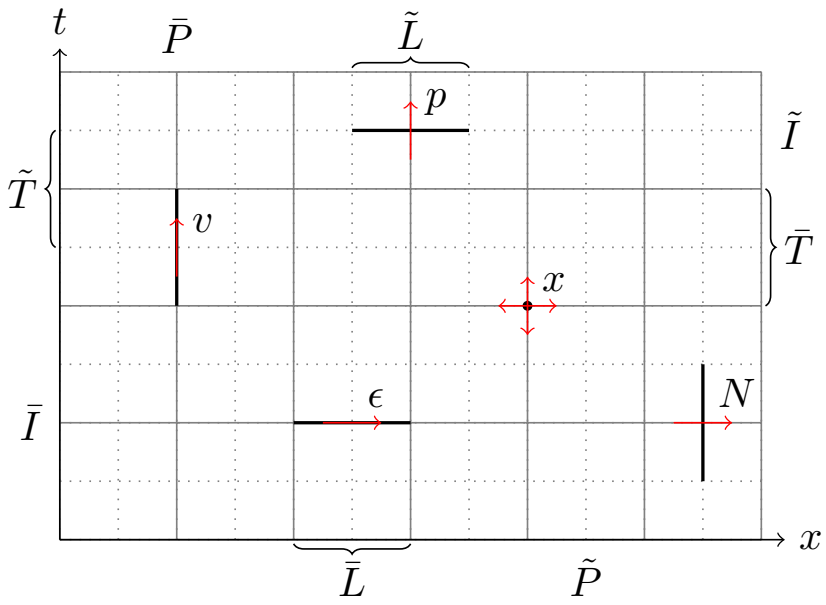

Figure 5.2: Discretised quantities p, x and N over temporal and spatial points and edges.

$$\int_a^b \int_0^T \left[\frac{p\delta p}{\rho A}\right] dt\, dx + \int_a^b \int_0^T \left[x\frac{\partial \delta p}{\partial t}\right] dt\, dx = 0 \quad \forall \delta p,$$

$$-\int_a^b \int_0^T \left[\frac{N\delta N}{EA}\right] dt\, dx - \int_a^b \int_0^T \left[x\frac{\partial \delta N}{\partial x}\right] dt\, dx = 0 \quad \forall \delta N,$$

$$\int_a^b \int_0^T \left[\delta x \left(\frac{\partial p}{\partial t} - \frac{\partial N}{\partial x}\right)\right] dt\, dx + \int_a^b \left[\delta x \lambda\Big|_0^T\right] dx + \int_0^T \left[\delta x \lambda\Big|_a^b\right] dt = 0 \quad \forall \delta x,$$

$$\int_a^b \left[(x - \hat{x})\, \delta\lambda\Big|_0^T\right] dx + \int_0^T \left[(x - \hat{x})\, \delta\lambda\Big|_a^b\right] dt = 0 \quad \forall \delta\lambda.$$

Following the discretisation of the variables p, x and N as described in [1] results in a discrete system that can thereafter be solved. p, x and N can be discretised as shown in Figure 5.2.

The extension of the time-dependent mimetic spectral element method to two-dimensional space for the wave equation follows by means of tensor products. Applications of this method are for instance a drum or a falling pebble in a well.

Explicitly stating that energy is not conserved is possible by adding a damper to the system, as is shown in Figure 5.1c. This field of studies is also open for exploration.

It needs to be said that all future work is still superficial and related to textbook problems. Thinking ahead and passed these textbook problems, the ultimate goal is to apply this time-dependent mimetic spectral element method to fluid dynamics. This incorporates for instance, convective terms.

A Full solution simple harmonic oscillator

Let the equation of motion be

$$m\ddot{x}(t) + kx(t) = 0. \tag{A.1}$$

Assume $x(t) = e^{rt}$ as a solution. Replace $\ddot{x}$ and x by its assumptions r^2e^{rt} and e^{rt} respectively. (A.1) is converted in

$$\begin{aligned} m\ddot{x}(t) + kx(t) &= 0, \\ mr^2e^{rt} + ke^{rt} &= 0, \\ \left(mr^2 + k\right)e^{rt} &= 0. \end{aligned} \tag{A.2}$$

As $e^{rt} \neq 0$, it follows that

$$mr^2 + k = 0 \tag{A.3}$$

must hold for it to be a solution to (A.1). Solving for r leads to

$$r = \sqrt{\frac{k}{m}}i \quad \vee \quad -\sqrt{\frac{k}{m}}i \tag{A.4}$$

and hence

$$\begin{aligned} x(t) &= c_1e^{\sqrt{\frac{k}{m}}ti} + c_2e^{-\sqrt{\frac{k}{m}}ti}, \\ &= c_1\left(\cos\left(\sqrt{\frac{k}{m}}t\right) + i\sin\left(\sqrt{\frac{k}{m}}t\right)\right) + c_2\left(\cos\left(\sqrt{\frac{k}{m}}t\right) - i\sin\left(\sqrt{\frac{k}{m}}t\right)\right), \\ &= d_1\cos\left(\sqrt{\frac{k}{m}}t\right) + d_2\sin\left(\sqrt{\frac{k}{m}}t\right). \end{aligned} \tag{A.5}$$

Here, (A.5) uses Euler's formula and $d_1 = (c_1 + c_2)$ and $d_2 = (c_1 - c_2)\,i$. With initial conditions $x(0) = x_0$ and $\dot{x}(0) = \dot{x}_0$ the solution becomes

$$x(t) = x_0\cos\left(\sqrt{\frac{k}{m}}t\right) + \dot{x}_0\sqrt{\frac{m}{k}}\sin\left(\sqrt{\frac{k}{m}}t\right). \tag{A.6}$$

Bibliography

[1] Enzo Tonti. On the mathematical structure of a large class of physical theories. Technical report, Politecnico di Milano (Italy) Instituto di Matematica, 1971.

[2] Jasper Kreeft, Artur Palha, and Marc Gerritsma. Mimetic framework on curvilinear quadrilaterals of arbitrary order. *arXiv preprint arXiv:1111.4304*, 2011.

[3] Enzo Tonti. *The mathematical structure of classical and relativistic physics*. Springer, 2013.

[4] Jozef Dodziuk. Finite-difference approach to the Hodge theory of harmonic forms. *American Journal of Mathematics*, 98(1):79–104, 1976.

[5] Alain Bossavit. Whitney forms: A class of finite elements for three-dimensional computations in electromagnetism. *IEE Proceedings A (Physical Science, Measurement and Instrumentation, Management and Education, Reviews)*, 135(8):493–500, 1988.

[6] Timo Tarhasaari, Lauri Kettunen, and Alain Bossavit. Some realizations of a discrete Hodge operator: a reinterpretation of finite element techniques [for EM field analysis]. *IEEE Transactions on magnetics*, 35(3):1494–1497, 1999.

[7] Claudio Mattiussi. A reference discretization strategy for the numerical solution of physical field problems. In *Advances in imaging and electron physics*, volume 121, pages 143–279. Elsevier, 2002.

[8] Jasper Kreeft, Artur Palha, and Marc Gerritsma. Mimetic spectral element method for generalized convection-diffusion problems. In *Proceedings of ECCOMAS CFD*. Portugal Lisbon, 2010.

[9] Pedro Pinto Rebelo, Artur Palha, and Marc Gerritsma. Mixed mimetic spectral element method applied to Darcy's problem. In *Spectral and High Order Methods for Partial Differential Equations-ICOSAHOM 2012*, pages 373–382. Springer, 2014.

[10] Bo Gervang, Kennet Olesen, and Marc Gerritsma. A Mimetic Spectral Element Method for Non-Isotropic Diffusion Problems. In *Spectral and High Order Methods for Partial Differential Equations ICOSAHOM 2016*, pages 229–242. Springer, 2017.

[11] Jasper Kreeft and Marc Gerritsma. A priori error estimates for compatible spectral discretization of the Stokes problem for all admissible boundary conditions. *arXiv preprint arXiv:1206.2812*, 2012.

[12] Jasper Kreeft and Marc Gerritsma. Mixed mimetic spectral element method for Stokes flow: A pointwise divergence-free solution. *Journal of Computational Physics*, 240:284–309, 2013.

[13] Artur Palha, Federico Felici, and Barry Koren. Mimetic spectral element method for the Grad-Shafranov equation. In *42nd European Physical Society Conference on Plasma Physics,(EPS 2015)*, pages P1–185. European Physical Society (EPS), 2015.

[14] Artur Palha, Barry Koren, and Federico Felici. A mimetic spectral element solver for the Grad–Shafranov equation. *Journal of Computational Physics*, 316:63–93, 2016.

[15] Marc Gerritsma, Artur Palha, Varun Jain, and Yi Zhang. Mimetic Spectral Element Method for Anisotropic Diffusion. In *Numerical Methods for PDEs*, pages 31–74. Springer, 2018.

[16] Mick Bouman. Mimetic Spectral Element Method for Elliptic Problems, 2010.

[17] Zeyu Liu. Preconditioning for Mimetic Spectral Element Method: A Preliminary Study Applied on Elliptic Equations. 2018.

[18] Artur Palha and Marc Gerritsma. Mimetic spectral element method for Hamiltonian systems. *arXiv preprint arXiv:1505.03422*, 2015.

[19] Joël Fisser. Advancing the Mimetic Spectral Element Method: Towards Continuum Mechanics Applications. 2019.

[20] Deepesh Toshniwal, Rene Huijsmans, and Marc Gerritsma. A geometric approach towards momentum conservation. In *Spectral and High Order Methods for Partial Differential Equations-ICOSAHOM 2012*, pages 393–402. Springer, 2014.

[21] Yi Zhang. Spatially mass-, kinetic energy-and helicity-preserving mimetic discretization of 3D incompressible Euler flows. 2016.

[22] Jerrold Eldon Marsden and Matthew West. Discrete mechanics and variational integrators. *Acta Numerica*, 10:357–514, 2001.

[23] Dina Razafindralandy, Aziz Hamdouni, and Marx Chhay. A review of some geometric integrators. *Advanced Modeling and Simulation in Engineering Sciences*, 5(1):16, 2018.

[24] Alain Jean Brizard. *An introduction to Lagrangian mechanics*. World Scientific Publishing Company, 2014.

[25] Ernst Hairer, Christian Lubich, and Gerhard Wanner. *Geometric numerical integration: structure-preserving algorithms for ordinary differential equations*, volume 31. Springer Science & Business Media, 2006.

[26] Serigne Bira Gueye, Kharouna Talla, and Cheikh Mbow. Solution of 1D poisson equation with neumann-dirichlet and dirichlet-neumann boundary conditions, using the finite difference method. *Journal of Electromagnetic Analysis and Applications*, 6(10):309, 2014.

[27] Charles Hirsch. *Numerical computation of internal and external flows: The fundamentals of computational fluid dynamics*. Elsevier, 2007.

[28] Paul L DeVries and Javier E Hasbun. *A first course in computational physics*. Jones & Bartlett Publishers, 2011.

[29] Anthony Ralston. Runge-kutta methods with minimum error bounds. *Mathematics of computation*, 16(80):431–437, 1962.

[30] Endre Süli and David F Mayers. *An introduction to numerical analysis*. Cambridge university press, 2003.

[31] Ernst Hairer, Christian Lubich, and Gerhard Wanner. Geometric numerical integration illustrated by the störmer–verlet method. *Acta numerica*, 12:399–450, 2003.

[32] Kolja Brix, Claudio Canuto, and Wolfgang Dahmen. Legendre-Gauss-Lobatto grids and associated nested dyadic grids. *arXiv preprint arXiv:1311.0028*, 2013.

[33] Marc Gerritsma. Edge functions for spectral element methods. In *Spectral and High Order Methods for Partial Differential Equations*, pages 199–207. Springer, 2011.

[34] Varun Jain, Yi Zhang, Artur Palha, and Marc Gerritsma. Construction and application of algebraic dual polynomial representations for finite element methods. *arXiv preprint arXiv:1712.09472*, 2017.

[35] John Ashworth Nelder and Roger Mead. A simplex method for function minimization. *The computer journal*, 7(4):308–313, 1965.